JGR Oceans

RESEARCH ARTICLE
10.1029/2018JC014840

# Hemispheric Asymmetry of the Pacific Shallow Meridional Overturning Circulation

**Mathias Zeller**[1,2], **Shayne McGregor**[1,3], **and Paul Spence**[3,4]

[1]School of Earth, Atmosphere and Environment, Monash University, Melbourne, Victoria, Australia, [2]ARC Centre of Excellence for Climate System Science, Sydney, New South Wales, Australia, [3]ARC Centre of Excellence for Climate Extremes, Sydney, New South Wales, Australia, [4]Climate Change Research Centre, University of New South Wales, Sydney, New South Wales, Australia

**Key Points:**
- The STC interannual variability is largely driven by ENSO-related winds
- We can attribute a crucial role to the winds nonlinearly related to ENSO which are not considered by the classic linear view of ENSO
- The decadal changes in the tropical Pacific after the Year 1993 appear to be mainly influenced by the Southern hemisphere STC

**Correspondence to:**
M. Zeller,
mathias.zeller@monash.edu

**Citation:**
Zeller, M., McGregor, S., & Spence, P. (2019). Hemispheric asymmetry of the Pacific shallow meridional overturning circulation. *Journal of Geophysical Research: Oceans*, *124*, 5765–5786. https://doi.org/10.1029/2018JC014840

Received 5 DEC 2018
Accepted 8 JUL 2019
Accepted article online 20 JUL 2019
Published online 15 AUG 2019

**Abstract** The shallow subtropical cells (STCs) in the Pacific Ocean are thought to modulate the background state that the El Niño-Southern Oscillation (ENSO) operates in. This modulation is proposed to impact the frequency and intensity of ENSO events and their teleconnections. We use a high-resolution ocean model to investigate the volume transports associated with the STC branches along 5° N and 5° S. We find three prominent differences between the Southern hemisphere (SH) STC and the Northern hemisphere (NH) STC: (i) the NH STC varies 26% stronger than the SH STC; (ii) the NH STC appears to lead the SH STC by 3 months which causes the NH and SH STCs to play different roles during the course of El Niño and La Niña events; and (iii) in spite of the relative symmetry of the wind stress trends, the STCs have differing decadal trends, with the SH STC clearly dominating the changes in the post-1993 period. To investigate the mechanisms driving the STC variability, we identify winds that are linearly and nonlinearly related to ENSO to force the ocean model. The hemispheric difference in interannual variance as well as the phase difference between the STCs can be explained with ENSO forcing. Our results suggest ENSO to be an important factor in modulating its own background state, with a prominent role for the winds that are nonlinearly related to ENSO. The decadal trends and their interhemispheric disparity, however, cannot be reproduced by our targeted ENSO experiments.

**Plain Language Summary** The tropical Pacific Ocean plays a key role in modulating the climate worldwide. It is home to the El Niño-Southern Oscillation (ENSO) which lets the ocean temperature rise and fall on time scales of a few years. The tropical Pacific Ocean also varies on time scales of a decade or longer, which is thought to influence the frequency, intensity, and potential predictability of ENSO. It is therefore important to understand the dynamics behind the decadal variability. The Pacific Ocean shallow circulation in the upper 200 m is assumed to be an important driver of the decadal changes in the tropical Pacific. Our study focuses on understanding the drivers of the Pacific Ocean shallow circulation. We conduct various experiments with an Ocean General Circulation Model using different wind forcings to investigate the role of specific wind patterns for the ocean circulation. We find prominent hemispheric differences of the shallow circulation that can be largely explained by wind forcing associated with ENSO. Most interestingly, we also find that changes associated with a phase change of the Pacific Decadal Oscillation in the Year 1993 appear to be largely induced by the Southern hemispheric circulation highlighting the importance of understanding the dynamics there.

## 1. Introduction

The tropical Pacific Ocean is the most influential region on climate patterns around the world (e.g., Alexander et al., 2002; Kosaka & Xie, 2013, 2016). This region houses the Earth's most prominent interannual climate variation, the El Niño-Southern Oscillation (ENSO; McPhaden et al., 2006). Besides the interannual variability of the coupled ocean-atmosphere system, the tropical Pacific Ocean also exhibits modulations on decadal time scales. The spatial pattern of these decadal modulations is captured by the Pacific decadal oscillation or the Interdecadal Pacific Oscillation, both of which describe recurring patterns of sea surface temperature (SST) and associated atmospheric conditions over the Pacific domain (e.g., Mantua et al., 1997; Power et al., 1999).

The decadal variability can be thought of as the background state upon which ENSO operates (Fedorov & Philander, 2001). Changes in this background state are thought to be closely linked to ENSO frequency and intensity (e.g., Zhao et al., 2016) as well as ENSO predictability by impacting the ocean dynamics that determine the lead-lag relationship between ENSO SST and its warm water volume (WWV) precursor (e.g., Neske & McGregor, 2018). Decadal changes in the tropical Pacific also serve as an explanation for the recent global warming hiatus (England et al., 2014). An enhanced understanding of the drivers of the decadal variability in this region is important for ENSO predictability and also for being able to distinguish between natural variability and human-induced climate change.

Details of what drives the decadal variability of the tropical Pacific Ocean are currently still debated (Newman et al., 2016). Atmospheric teleconnections between the extratropics and the tropics (e.g., Barnett et al., 1999; Kwon et al., 2011) and between ocean basins (e.g., Chikamoto et al., 2016; McGregor et al., 2012) may explain some portion of the decadal signal in the tropics. The focus of this study will be on the oceanic teleconnections between the extratropics and the tropics as important drivers of the tropical variability. We will investigate the oceanic teleconnections with emphasis on both the interannual and the decadal time scales as they both play a role in modulating the tropical Pacific climate.

Two oceanic mechanisms connecting the tropical and extratropical Pacific ocean can be distinguished. They are (i) the vertically integrated exchanges of upper ocean mass/heat that modulate the WWV of the equatorial Pacific Ocean and (ii) the shallow ocean circulation cells, known as the Pacific subtropical cells (STCs), that extend from the tropics to the subtropics in both hemispheres and form part of the global ocean circulation system (Lee & Fukumori, 2003; Liu et al., 1994; McCreary & Lu, 1994; Schott et al., 2004). WWV changes are normally utilized when discussing the dynamics of ENSO events (e.g., Kug et al., 2003; Jin, 1997; McGregor et al., 2014), while the Pacific STCs, which are the focus of this study, are generally used when discussing mechanisms of Pacific Decadal variability (e.g., Johnson & McPhaden, 1999) which is strongly related to the volume and temperature of the water upwelled in the equatorial region. Each of the STCs is made up of different branches which can behave independently of each other (e.g., Capotondi et al., 2005). In the subtropics, cold water is subducted into the thermocline at depth from where it makes its way toward the tropics (Johnson & McPhaden, 1999). Two distinct pathways for the subsurface limb have been explored, one along the western boundary as a western boundary current (WBC) and one through the ocean interior away from any boundaries (Izumo et al., 2002; Liu et al., 1994). At the equator, the water is upwelled along the equatorial undercurrent (EUC), before the overlying trade winds cause the upwelled water to diverge in poleward direction closing the loop (e.g., Johnson, 2001). It should be noted that the two mechanisms are not entirely independent of each other. When the STC branches vary in phase, the spin rate of the STCs increases or decreases impacting the rate of equatorial upwelling while having no effect on the WWV. When the STC branches vary out of phase, however, the STCs contribute to upper ocean heat exchanges and therefore changes in WWV.

Most studies separate the equatorward STC transport into an ocean interior transport and a WBC transport (e.g., Capotondi et al., 2005; Cheng et al., 2007; Hong et al., 2014; Lee & Fukumori, 2003; Lbbecke et al., 2008). In all of these studies, the WBC opposes the interior transport at both interannual and decadal time scales. This leads to a partial compensation of the interior flow given that the WBC does not vary as much as the interior transports. A study by Ishida et al. (2008) identifies asymmetries in integrated upper ocean transport between the Northern hemisphere (NH) and the Southern hemisphere (SH) on ENSO time scales. Using a high-resolution ocean model, the authors explain this asymmetry by indicating that the compensation between the interior and the WBC transports is higher in the SH than in the NH and that the limited compensation in the NH is underpinned by a phase lag between the WBC transports and the interior transports. However, Ishida et al. (2008) do not distinguish between surface and subsurface interior transports. The present study builds on the Ishida et al. (2008) study by looking at hemispheric asymmetries of the branches related to the STCs. The distinction of the vertical distribution of volume transport enables us to more accurately identify the reason for the hemispheric asymmetry in STC transports and relate the timing of the branches back to the forcing.

Hemispheric asymmetries of the STC transports can have a substantial climatic impact in the equatorial Pacific. Given the strong difference in mean pycnocline ($\sigma_{24}$–$\sigma_{26}$) temperatures (Figure 1) between the NH (roughly 17–22 °C) and SH (roughly 21–24 °C), the relative contribution of each hemisphere's STC

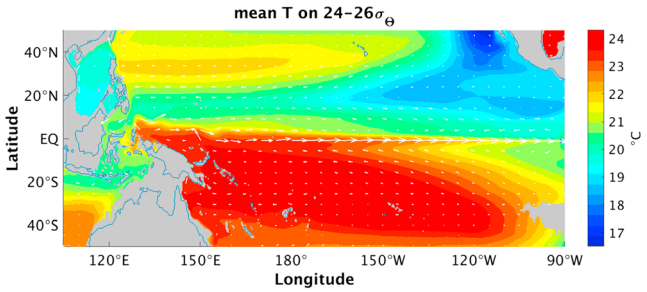


**Figure 1.** Time mean temperature averaged over the $\sigma_{24}$–$\sigma_{26}$ isopycnal surfaces in the MOM025 control experiment.

pycnocline transport has the potential to strongly influence the temperature of the water that is transported in the EUC and is then upwelled at the equator.

The STCs have been proposed to impact the decadal variability of the tropical Pacific Ocean in several ways. Early studies proposed that the equatorward advection of subducted temperature anomalies within the STCs play an important role (Giese et al., 2002; Gu & Philander, 1997; Zhang et al., 1998). However, other studies found that subducted North Pacific temperature anomalies are dispersed before reaching the equator (Hazeleger, Visbeck, et al., 2001; Schneider, Miller, et al., 1999, Schneider, Venzke, et al., 1999). According to Luo and Yamagata (2001), the advection of temperature anomalies from the subtropics to the tropics might still be effective in the SH. An alternative mechanism suggests that the anomalous STC volume transports can modulate the amount of cold subsurface waters that is advected into the tropics and upwelled to the surface along the equator where it interacts with the overlying atmosphere (Kleeman et al., 1999).

In support of the aforementioned theory, the different branches of the STCs have been found to strongly vary on interannual time scales (Capotondi et al., 2005; Izumo, 2005; Lee & Fukumori, 2003; Schott et al., 2007, 2008), whereby the STCs are closely linked to the ENSO cycle, with decreased overturning transport during El Niños and enhanced meridional transport during La Niñas (Izumo, 2005; McPhaden & Zhang, 2002). On decadal time scales, McPhaden and Zhang (2002) observed a decrease of the STC convergence at the thermocline depth of 11 Sv between the 1970s and 1990s at 9° N and 9° S, followed by a substantial increase of about 10 Sv between the 1990s and the early 2000s (Feng et al., 2010; McPhaden & Zhang, 2004). Some studies expanded on this by including the trends of the WBC, resulting in much weaker decadal trends of the basin-wide STC thermocline convergence than previously assumed (Lee & Fukumori, 2003; Schott et al., 2007; Lee & McPhaden, 2008). It should be noted, here, that the interannual variability of the STC branches is directly linked to the STC's decadal variability, for example, through the interannually varying level of compensation between the WBC and the subsurface interior transport.

To draw conclusions on decadal changes in the tropical Pacific, we, therefore, ascribe importance to the understanding of both the interannual and the decadal variabilities of the STCs. There are several hypotheses as to what drives the STC interannual and decadal variabilities. They all agree on the surface winds being the driving force; however, what differs between these hypotheses is the location and the pattern of these winds. Nonaka et al. (2002), Lee and Fukumori (2003), Capotondi et al. (2005), and Izumo (2005) emphasize the importance of local (tropical) wind stress and wind stress curl for transport variations of the STC. In contrast, Kleeman et al. (1999) highlight the role of remote (off-equatorial) winds poleward of 23°. Farneti et al. (2014) and McCreary and Lu (1994) also point out the role of off-equatorial winds; however, they identify those that occur between about 15° and 18° latitude as the primary driver of the low-frequency STC variability. The present study intends to identify the forcing of the individual STC branches (surface, subsurface interior, and WBC) in each hemisphere as they may have distinct roles in impacting the decadal variability of the tropical Pacific. A particular focus of this study will be on the winds related to ENSO dynamics, following the idea that ENSO variability potentially self-regulates its low-frequency background variations.

In this regard, a study of particular interest reveals a combination mode where the interannual (ENSO) and seasonal SST variabilities in the tropical Pacific form a nonlinear response in the atmospheric circulation (Stuecker et al., 2013). The corresponding circulation pattern features an anomalous Philippine anticyclone in the Northwestern tropical Pacific as well as a southward shift of westerly wind anomalies to the Southeastern tropical Pacific. Both features together result in a strong meridional shear of anomalous zonal wind across the equator. This atmospheric circulation, which has a nonlinear relation to ENSO, has been shown in previous studies to play a prominent role in the vertically integrated exchanges of upper ocean heat related to ENSO (McGregor et al., 2014). However, its role in driving STC changes has yet to be fully explored. The present study aims to qualitatively and quantitatively assess the contribution of the transports induced by the nonlinear atmospheric forcing to the tropical Pacific overturning circulation.

Thus, in this study, we are not so much interested in how the STCs impact the tropical Pacific on decadal time scales but more in what drives the STCs on both interannual and decadal time scales as we think it is

important to first understand the dynamics behind the STC variability. As a next step, it is naturally worth to look at the actual impact of the STCs on the tropical climate. We investigate the physical mechanisms driving the STCs on interannual and decadal time scales, also asking how much ENSO itself can drive the modeled STC variability. For our analysis, we distinguish between winds that are linearly related to ENSO and non-linearly related to ENSO (combination mode). The fact that we make use of a high-resolution ocean general circulation model that resolves mesoscale variability in the tropics and subtropics enables us to realistically simulate the ocean's complex eddy structures at the Western boundary and tropical instability waves. It also allows for a separation of the different branches of the STCs that we expect to be more consistent with observations, specifically to distinguish between the WBC and the ocean interior flow. In previous studies, this distinction was hampered by a coarse model resolution (Capotondi et al., 2005; Izumo, 2005).

The paper is structured as follows: In section 2, the ocean general circulation model as well as the wind forcing and the experimental setup are described. Section 3 gives an overview of the results, including the analysis of the covariability between the STC branches at interannual and decadal time scales as well as the comparison of the ENSO forced experiments. Conclusions are discussed in section 4.

## 2. Model and Methods

### 2.1. The Ocean Model

The GFDL-MOM025 global coupled ocean sea-ice model is used for the analysis (Spence et al., 2014). This model is based on the GFDL CM2.5 coupled climate model (Delworth et al., 2012) and is coupled to the GFDL Sea Ice Simulator model. It has a 1/4° Mercator horizontal resolution globally with 50 vertical levels. The vertical level thicknesses range from 10 m at the surface to about 200 m at depth. Sea surface salinity is restored to a seasonally varying climatology on a 60-day time scale. The model is equilibrated with a 40-year spin-up control simulation forced with the ERA-interim climatology of heat, freshwater, and momentum fluxes. Output is given as 5-day averages.

### 2.2. The Forcing

The ocean model is forced with atmospheric conditions derived from the European Centre for Medium-Range Weather Forecasts (ECMWF) ERA-interim reanalysis product (Dee & Uppala, 2009). The atmospheric conditions are converted to heat, freshwater, and momentum fluxes across the ocean surface using the bulk formulas. The forcing spans a time period of a bit more than 37 years from January 1979 to May 2016. Hence, the buildup phase of the most recent strong El Niño event of 2015/2016 is included and could be used for the analysis. The ERA-interim winds were selected to overcome the strong trend biases in wind stress and wind stress curl over the tropical Pacific that are known to be present in the National Center for Environmental Prediction wind product (McGregor et al., 2012). McGregor et al. (2012) found the spatial trend pattern of sea surface height (SSH) anomalies derived from National Center for Environmental Prediction winds to have a much lower spatial correlation (0.41) when compared with observed SSH anomalies than those derived from ERA-interim winds (0.83). It is noted that this choice moved us away from the more balanced fluxes of CORE forcing (Large & Yeager, 2009), but it is more appropriate to address the proposed research questions.

### 2.3. The Experiments

We performed four experiments which are analogous to those of McGregor et al. (2014) and extended them to 2016. The experiments all use the same climatological heat and freshwater forcing, but they differ in their wind forcing. Experiment 1 is referred to as $EXP_{\mathrm{FULL}}$ as it is forced with the full ERA-interim wind field. For the three ENSO-targeted experiments, the idea is to decompose the complex ocean dynamics response to ENSO into several more digestible components that are more intuitive and easier to understand. The decomposition is done on the equatorial Pacific surface wind stress forcing utilizing linear regression and an Empirical Orthogonal Function (EOF) analysis. Prior to this, wind velocities are converted to wind stresses according to the quadratic stress law

$$\begin{pmatrix} \tau_x \\ \tau_y \end{pmatrix} = C_{\mathrm{d}} \rho_{\mathrm{a}} \begin{pmatrix} u \\ v \end{pmatrix} W, \tag{1}$$

where $\tau_x$ and $\tau_y$ are the horizontal wind stresses, $C_{\mathrm{d}}$ is the drag coefficient ($C_{\mathrm{d}} = 1.5e^{-3}$), $\rho_{\mathrm{a}}$ is the reference atmospheric density ($\rho_{\mathrm{a}} = 1.2\ \mathrm{kg/m^3}$), $u$ and $v$ are the horizontal wind velocities, and $W$ is the surface wind speed.

Experiment 2 only utilizes wind stress anomalies that are linearly related to the ENSO cycle. This is achieved by regressing global wind stresses onto the Nino3.4 time series which is a direct indicator of the ENSO phase

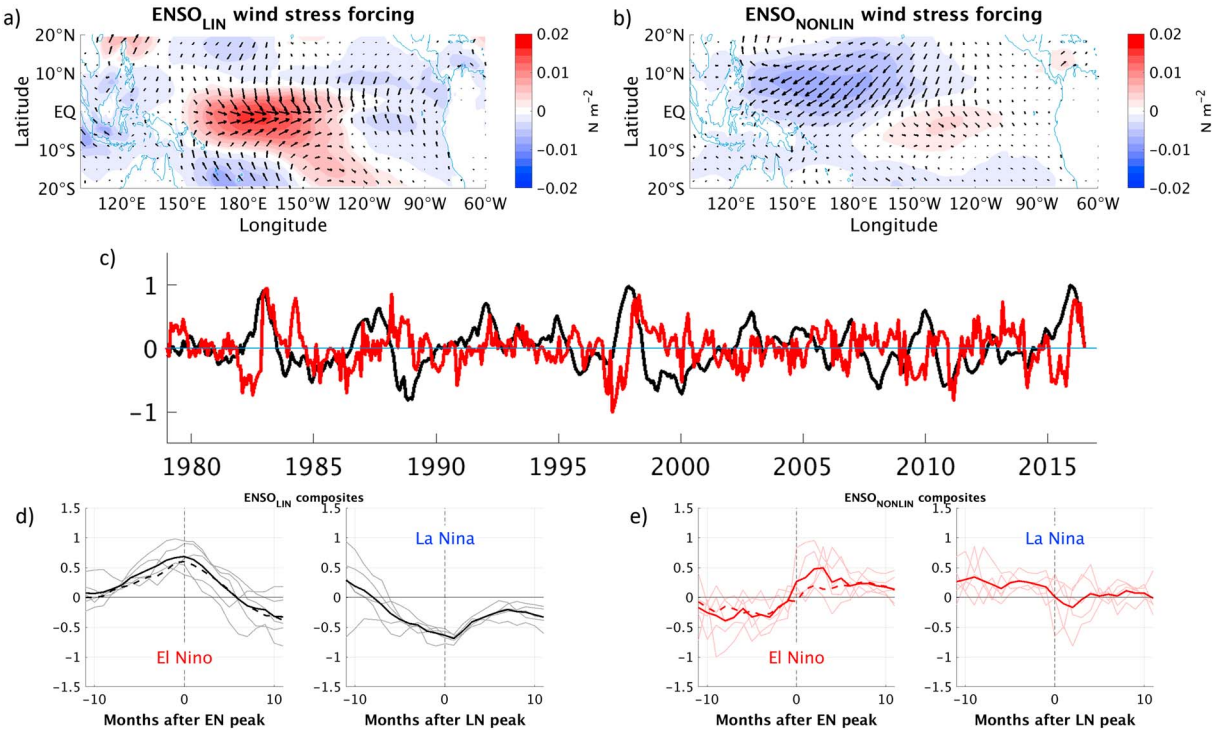


**Figure 2.** Wind stress patterns that are (a) linearly related to ENSO ($ENSO_{LIN}$, linear regression against Nino3.4 index) and (b) nonlinearly related to ENSO ($ENSO_{NONLIN}$, EOF2 of equatorial wind stresses). The zonal component is shaded where red means eastward. (c) Time evolution of $ENSO_{LIN}$ (black) and $ENSO_{NONLIN}$ (red) wind stress forcings. (d) and (e) show the composite mean time series around Eastern Pacific El Niño (solid, 1982/1983, 1987/1988, 1991/1992, 1997/1998, and 2002/2003), Central Pacific El Niño (dashed, 1994/1995, 2004/2005, 2009/2010, and 2015/2016), and La Niña (1988/1989, 1998/1999, 1999/2000, 2007/2008, and 2010/2011) events for $ENSO_{LIN}$ and $ENSO_{NONLIN}$ wind stresses, respectively. Transparent lines show the single events. All time series are normalized, and the patterns are standardized with the standard deviation of their time evolution. ENSO = El Niño-Southern Oscillation.

(SSTs are derived from ERSST (Extended Reconstructed Sea Surface Temperature) version 4). As the Nino3.4 index is very close to the first Principle Component (PC1) time series of wind stresses within the equatorial Pacific region (120° E–60° W, 10° N–10° S, corr = 0.71; cf. McGregor et al., 2014), the resulting regression map largely coincides with the first EOF of the same region (spatial corr: 0.93). Due to its linear relationship with ENSO, the experiment is named $ENSO_{LIN}$ (Figures 2a and 2c).

Experiment 3 utilizes wind stress anomalies that have a nonlinear relationship with ENSO. To this end, we first subtract wind stress anomalies related to $ENSO_{LIN}$ from the $EXP_{FULL}$ wind stress anomalies, globally. We then compute the first EOF of the residual wind stress in the tropical Pacific region (120° E–60° W, 10° N–10° S). This EOF is very similar to the EOF2 of the original wind stress field (PC corr: 0.83; spatial corr: 0.92) The resulting principle component time series (Figure 2c) is finally regressed onto the global residual wind stress field to obtain the associated global structure (Figure 2b). As these wind stress anomalies are known to be nonlinearly related to ENSO (Stuecker et al., 2013), this experiment is termed $ENSO_{NONLIN}$.

Experiment 4 uses the sum of $ENSO_{LIN}$ and $ENSO_{NONLIN}$ wind stress anomalies. It is therefore referred to as $ENSO_{ALL}$ and includes all wind stresses that are related to ENSO. To produce the final wind forcing of each of the aforementioned experiments, the wind stress anomalies of $ENSO_{LIN}$, $ENSO_{NONLIN}$, and $ENSO_{ALL}$ are each added to the wind stress climatology and converted back to wind velocities.

Except where explicitly stated differently, for all our analysis, we compute 12-month moving averages of anomalies with respect to the mean seasonal cycle and the linear trend of the period January 1979 to May 2016. All correlations and linear trends are significant at the 90% confidence level unless indicated otherwise. Significance is computed using a bootstrap method with 10,000 iterations. To account for the monthly dependence of the data, a reduced number of degrees of freedom has been applied. Assuming that any one year (January–December) is independent of all other years, we divide the time series into yearly chunks of 12 months length. Each bootstrap sample time series is created by sampling with replacement from the 37 individual years. The resulting time series is then correlated with the second time series of interest. Given 37 years of model data, this leaves us with 37 degrees of freedom.

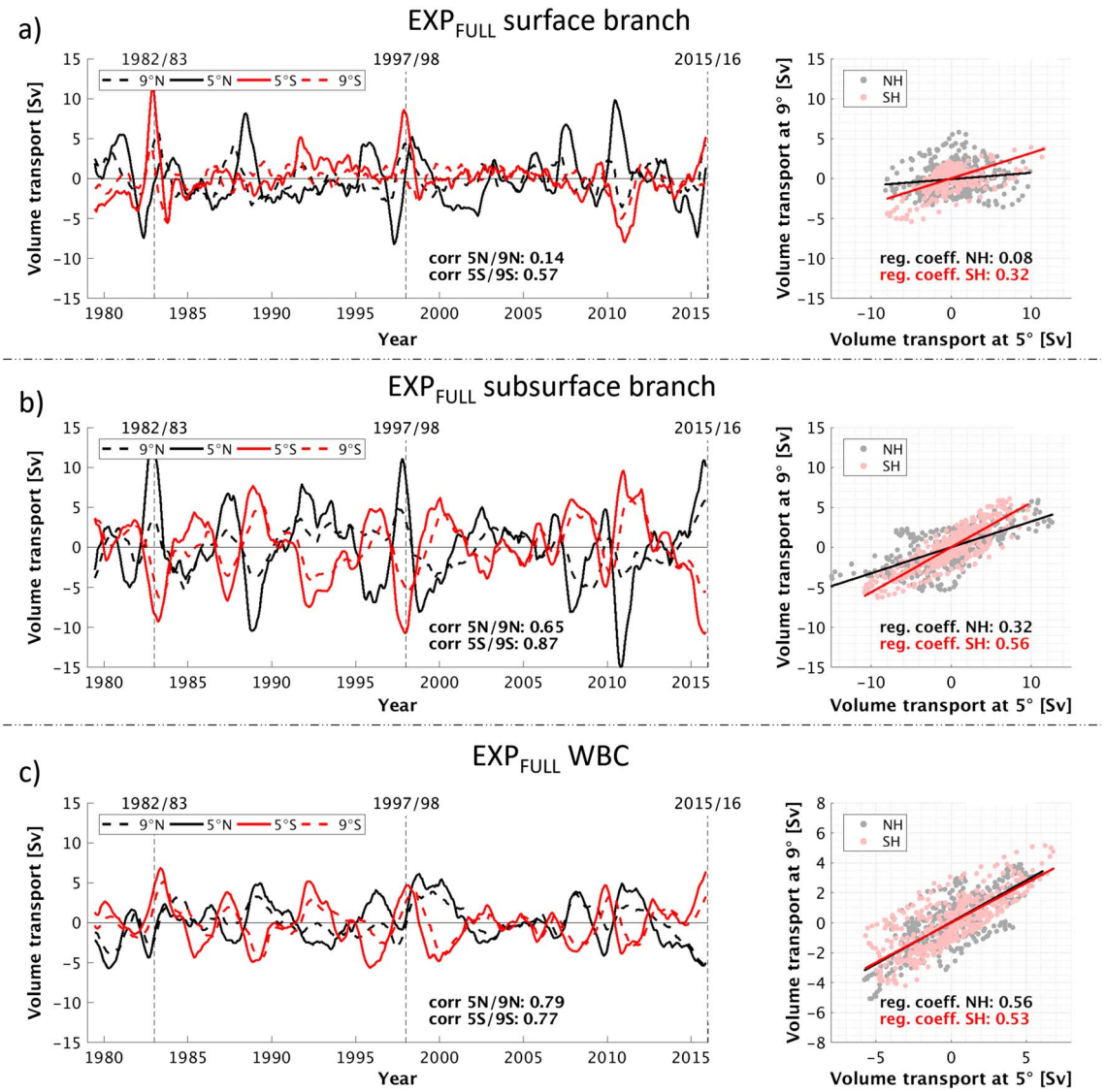


**Figure 3.** Transport anomalies of (a) the surface branch, (b) the subsurface interior branch, and (c) the WBC in $EXP_{FULL}$. Transports integrated across 5° N (solid black), 5° S (solid red), 9° N (dashed black), and 9° S (dashed red) are plotted as time series and as scatter plots. The vertical dashed black lines indicate the strong El Niño events of 1982/1983, 1997/1998, and 2015/2016. Positive means northward transport. The correlation between 5° N and 9° N in (a) is insignificant at the 90% confidence level. NH = Northern hemisphere; SH = Southern hemisphere; WBC = western boundary current.

### 2.4. Definition of the STC Branches

The STCs are defined on the time mean as this is where these cells are most clearly identified. Bearing in mind that the STC transports change with the distance from the equator, we choose 5° latitude for two main reasons: (i) We want to capture the strong and meridionally close to uniform zonal winds corresponding to the linear theory of the buildup and decay of El Niño events, and (ii) we want to be reasonably close to the equator, without interfering with the equatorially confined tropical cells, to ensure that the equatorward flow of pycnocline water across this latitude band actually feeds the EUC which then distributes the water to the surface at the equator. Another advantage of choosing 5° latitude is the opportunity to compare our results to other model studies (e.g., Izumo, 2005) as well as observational studies (e.g., Meinen & McPhaden, 2000; Meinen et al., 2001). In spite of this, questions still remain over whether 5° latitude is an adequate latitude to examine the STCs (Hazeleger, De Vries, et al., 2001) given the possible existence of tropical cells that recirculate equatorial waters in a meridionally narrower and shallower cell than the STCs do (e.g., Hazeleger, De Vries, et al., 2001; Izumo, 2005). However, these studies show that tropical cell downwelling occurs at 3–5° latitude while the major horizontal flow of these cells occurs between 1° and 3° latitude.

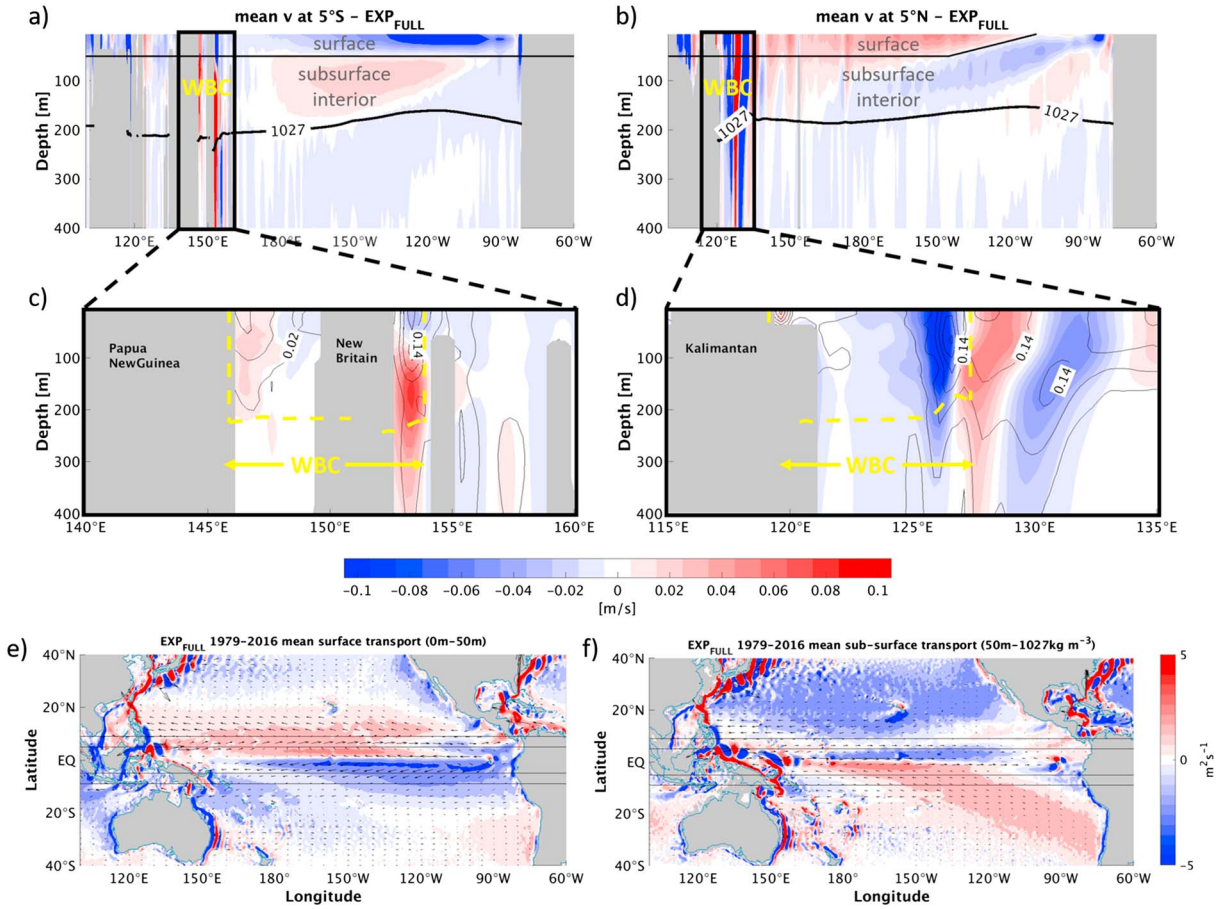


**Figure 4.** Mean meridional velocity ($v$) along 5° S (a) and 5° N (b), in the upper Pacific Ocean in $EXP_{\mathrm{FULL}}$. (c) and (d) are enlargements of the respective Western boundary regions. Mean of January 1979 to May 2016. Red shading means northward flow. The horizontal black line indicates the lower vertical boundary of the surface branch at 50 m (except slope at 5° N). The curved solid black line indicates the lower vertical boundary of the subsurface branch at $\sigma_{27}$. Note that the velocities need to be multiplied by 5 in (c) and (d). Black contours in (c) and (d) indicate the std of $v$. The contour interval is 0.4 m/s. (e) and (f) show maps of mean transport (meridional transport is shaded) integrated across the surface layer (0–50 m) and the subsurface layer (50 m–$\sigma_{27}$), respectively. The horizontal lines indicate the 5° and 9° latitudes in each hemisphere. WBC = western boundary current.

Thus, the predominant portion of the transports across 5° latitude form part of the STCs and therefore also constitute source water of the EUC. This is corroborated by the high coherence of the individual branches at 5° and 9° latitude (Figure 3). An exception is the NH surface branch which behaves very differently between the two latitudes, a fact that is also expressed in the insignificant correlation between the two latitudes. The different behavior can be explained with the wind forcing (Figures 2a and 2b). At 9° N, the surface branch is almost exclusively forced by the $ENSO_{\mathrm{NONLIN}}$ winds with no contribution by the $ENSO_{\mathrm{LIN}}$ winds, while at 5° N, both forcings play a role.

For the time mean in $EXP_{\mathrm{FULL}}$, the vertical structure of the meridional flow in the tropical Pacific shows a clear distinction between the surface and the subsurface (Figures 4a and 4b). At the surface, the water is largely diverging from the equator following Ekman dynamics induced by the overlying easterly trade winds (Figure 4e). At the subsurface, the basin-wide barotropic zonal pressure difference induces geostrophic convergence (Figure 4f). As a separation between the surface and subsurface branches, most studies use the 50-m level, sometimes combined with the 1,022 kg/m$^3$ isopycnal (e.g., Capotondi et al., 2005; Izumo, 2005; Lee & Fukumori, 2003). Figure 4 shows that at 5° S, the 50-m level seems adequate, so we use this as the boundary between the surface and subsurface branches. At 5° N, however, the surface Ekman flow seems to be confined to the basin interior with no transport east of 105° W. Instead, the equatorward subsurface flow rises to the surface between 145° and 105° W. To adapt to the changing surface-subsurface boundary, we choose the 50-m level west of 145° W and introduce a linear slope east of 145° W that reaches the surface at 105° W. East of this longitude, our definition accounts for no surface branch but only a subsurface branch.

To further separate the subsurface branch from the deep ocean, we use the 1,027 kg/m$^3$ isopycnal ($\sigma_{27} = \rho_{1027} - 1,000$ kg/m$^3$) as the lower boundary. In comparison with the ORAS4 (Ocean Reanalysis System version 4) reanalysis, the depth of the model's $\sigma_{27}$ is about 20 m shallower, and the pycnocline appears to be slightly narrower in the model. However, depths of neutral density levels (not shown) along which geostrophic flow is assumed to occur are very close to observations at 5° N and 5° S (Johnson & McPhaden, 1999). Moreover, the integration depth of 150–250 m is in the same range as in earlier studies (e.g., Capotondi et al., 2005; Izumo, 2005; Lee & Fukumori, 2003; 150–300 m), and importantly, the subsurface transport integration occurs over the range of isopycnals feeding the EUC (100–250 m).

Model studies have shown that there exist two main pathways for the equatorward pycnocline flow, one along the western boundary and one through the interior ocean (e.g., Capotondi et al., 2005; Lee & Fukumori, 2003; Liu et al., 1994). As the WBC is subject to different dynamics than the interior flow, it is defined here as a separate branch. To be consistent with the vertical extent of the interior transport, the WBC is integrated from the surface down to $\sigma_{27}$ (Figures 4c and 4d). The actual WBC reaches depths of about 1,000 m, which is much deeper than what we include here; however, the transports according to both definitions have a very similar variability and only differ in their mean and slightly in their standard deviation (not shown). Considering that we are interested only in the anomalies justifies our definition.

Another issue is the longitudinal extent of the WBC. Owing to the lack of a continuous continental shelf in the western Pacific, we define the western edge of the western boundary region manually at each latitude such that it includes the WBC but not any currents west of that. This distinction is especially important around the equatorial region where the impact of the Indonesian Throughflow (ITF) becomes large. It is important to note that the ITF is defined as its own branch and is differentiated from the STCs. It was shown that the presence or absence of the ITF does not considerably impact the STC transports (Lee & Fukumori, 2003).

To separate the WBC from the ocean interior, we define a "core" WBC at each latitude, which is defined as the meridional transport integrated across 3° longitude and vertically integrated from the surface to $\sigma_{27}$. The core WBC is then correlated with the vertically integrated meridional transport at each longitude. Based on this method, the eastern edge of the WBC is defined as the last longitude (from west to east) before the correlation crosses the zero line. From this analysis, we get the following widths for the WBC at the respective latitude: 8.25° at 5° N and 8° at 5° S. Interior transports are, thus, defined as everything east of the western boundary until the eastern coastline of the Pacific. This applies for both surface and subsurface branches.

In order to examine the variability of the STCs, we define an index of the combined NH and SH STC transports. We integrate the meridional velocity horizontally and vertically according to the above definition of the STC branches. The STC index is then computed as follows:

$$\begin{aligned} STC_{\mathrm{idx}} &= STC_{\mathrm{NH}} + STC_{\mathrm{SH}} \\ &= (SFC - SUB - WBC)_{\mathrm{NH}} + (SUB + WBC - SFC)_{\mathrm{SH}}, \end{aligned} \tag{2}$$

where *SFC*, *SUB*, and *WBC* denote the surface, subsurface, and WBC branches, respectively, of the STC. NH and SH refer to the NH and SH, respectively.

### 2.5. Model Validation

The model mean state of the tropical Pacific is very close to the ORAS4 reanalysis with high spatial correlations of sections across 5° N/5° S for mean meridional velocity (0.75/0.95) and mean density (0.99/0.996). The mean STC strength in the $EXP_{\mathrm{FULL}}$ control experiment is stronger in the SH (35 Sv) than in the NH (29 Sv), This is consistent with Lohmann and Latif (2005) who found the overturning to be 40 and 25 Sv for the SH and NH STC at the same latitudes, respectively, using a stream function to define the STC index. Table 1 shows a comparison of the model versus observed mean STC transports. The mean Ekman divergence of 49 Sv is comparable to but somewhat weaker than the one calculated from ERS-1,2 scatterometer wind stresses (58 Sv) across the same latitudes (Schott et al., 2004). In terms of the boundary currents, the mean SH WBC is measured at 15 Sv using gliders (Davis et al., 2012), while the model mean of 8.1 Sv is only about half. Butt and Lindstrom (1994) observed the SH WBC to mainly occur through the straits between Papua New Guinea and New Britain and between New Britain and New Ireland, which is consistent with our model (cf. Figure 4c). In the NH, Wijffels et al. (1995) used Accoustic Doppler Current Profilers (ADCPs) to measure the Mindanao Current to be 23 Sv on average of which 9 Sv turn west and form part of the ITF (Gordon et al., 1999), while the

**Table 1**
*Model Versus Observed Mean Transports of Surface, Subsurface Interior, and WBC Branches of the Subtropical Cells at 5° S and at 5° N*

| STC Branches | $EXP_{FULL}$ | Observations |
|---|---|---|
| Ekman divergence | 49 | 58 |
| NH WBC | −14.4 | −14 |
| SH WBC | 8.1 | 15 |
| NH interior | −3.2 | −5 |
| SH interior | 10.6 | 15 |

*Note.* Units are in Sverdrup. Positive means northward transport. WBC = western boundary current; NH = Northern hemisphere; SH = Southern hemisphere.

remaining 14 Sv feed the EUC (Johnson & McPhaden, 1999). The latter number coincides with the modeled 14 Sv of the mean NH WBC. An observational validation of the mean SH subsurface interior transports (Figure 4a) is given by Zilberman et al. (2013) who observed meridional geostrophic velocity derived from Argo floats at 7.5° S (their Figure 3a). Spatially, the mean subsurface transports extend from 170° E to 90° W, both in the model and in the observations. Also, the vertical extent of the mean equatorward transports compares well between model and observations, reaching down to a maximum of about 200 m between 170° and 150° W and shoaling toward the east reaching the 50-m level at about 100° W. Zilberman et al. (2013) observe an amplitude of 5 cm/s for the geostrophic velocity below the 50-m level which is slightly higher than the modeled amplitude of 4 cm/s for the subsurface branch. The strong southward velocity simulated at the Eastern boundary was also detected by the Argo floats and corresponds to the Peru-Chile Undercurrent as discussed by Montes et al. (2010, their Figures 3c and 3d). The integrated mean equatorward interior transports in $EXP_{FULL}$ amount to 3.2 and 10.6 Sv for the NH and SH, respectively. This is in qualitative agreement with the observed transports by Johnson and McPhaden (1999) amounting to 5 and 15 Sv, respectively, although with reduced magnitude.

The interannual variability of the model upper ocean transport (surface to pycnocline) at 9° latitude is comparable to the observed Ekman and geostrophic transports across 8° latitude in Meinen and McPhaden (2001, their Figure 9) showing similar peaks around ENSO events. The modeled temporal evolution of the STC subsurface branches at both 5° and 9° latitude is also consistent with the geostrophic transports calculated by Bosc and Delcroix (2008) from observed sea level anomalies at 5° and 8° latitude. However, the amplitude of the modeled STC transport at 5° and 9° latitude is about half compared to the observations.

## 3. Results

### 3.1. STC Index Variability

The fully forced ($EXP_{FULL}$) STC index calculated at 5° latitude exhibits large temporal variations of up to ±30 Sv (mean: 73 Sv), especially around El Niño and La Niña events (Figure 5a). During El Niños, the STCs slow down, meaning that less subtropical water intrudes the tropics and is upwelled along the equator. Also, at the surface, less water escapes from the tropical region. This process is reversed during La Niñas when the STCs are strong and lead to an increase of subtropical water in the tropical region.

A good agreement exists with the $ENSO_{ALL}$ STC index explaining 56% of the $EXP_{FULL}$ STC index (corr: 0.75, Figure 5b). $ENSO_{ALL}$ reaches about $\frac{2}{3}$ of the standard deviation of $EXP_{FULL}$. Further breaking down the forcing shows that the linear wind stress forcing seems to play the dominant role explaining 85% of $ENSO_{ALL}$. The $ENSO_{NONLIN}$ STC index explains 37% of $ENSO_{ALL}$ and shows clear peaks during ENSO events, also suggesting a nonnegligible role for $ENSO_{NONLIN}$.

On decadal time scales, the STC index also shows some variation which can be represented by the two linear trends before and after the observed phase shift in the tropical Pacific in the mid-1990s (McPhaden & Zhang,

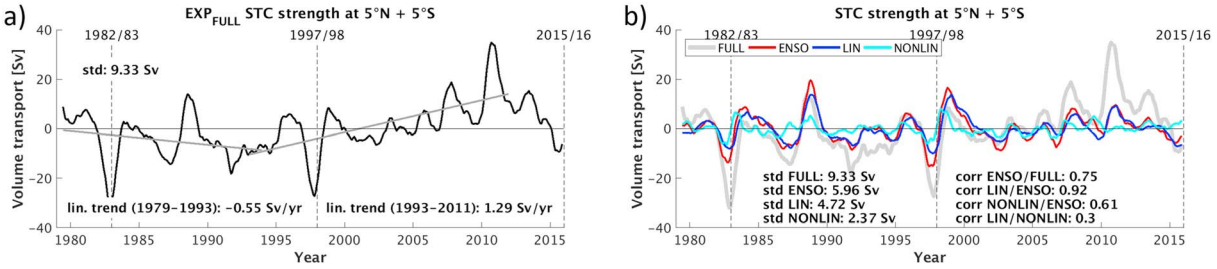


**Figure 5.** (a) Anomalies of STC strength at 5° N + 5° S for $EXP_{FULL}$. The linear trend for the period January 1979 to May 2016 has not been removed here. The linear trends for the periods 1979–1993 and 1993–2008 are plotted as gray lines; however, the linear trend in the earlier period is insignificant at the 90% confidence level. The standard deviation and the linear trends are displayed in the plot. (b) Anomalies of STC strength at 5° N + 5° S. Gray color denotes $EXP_{FULL}$, red $ENSO_{ALL}$, blue, $ENSO_{LIN}$, and cyan $ENSO_{NONLIN}$. The vertical dashed black lines indicate the strong El Niño events of 1982/1983, 1997/1998, and 2015/2016. Positive means anomalously strong STC. STC = subtropical cell; ENSO = El Niño-Southern Oscillation.

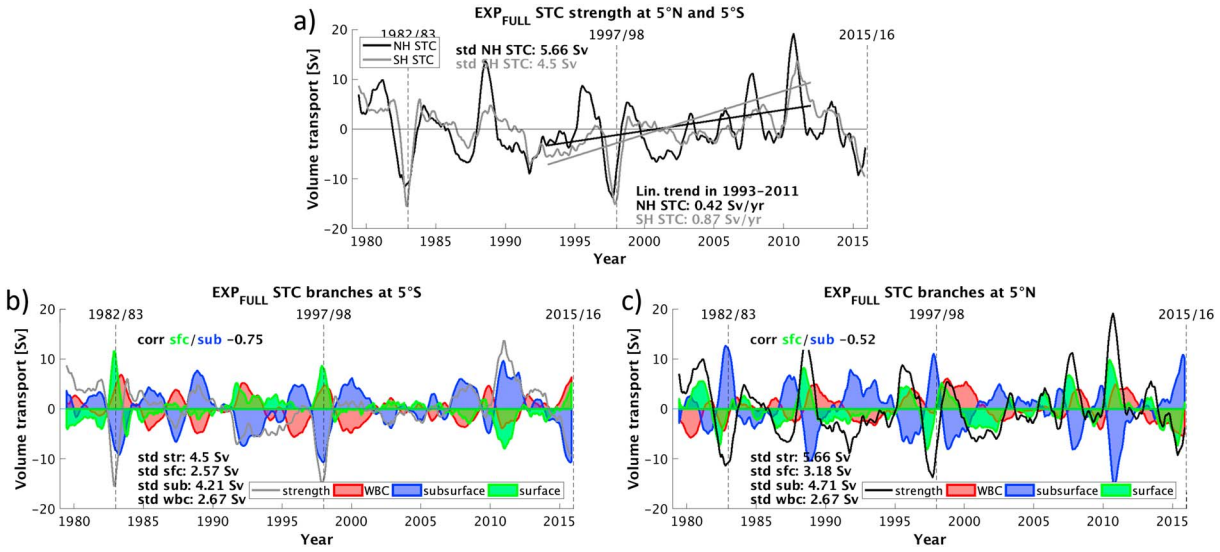


**Figure 6.** (a) Anomalies of STC strength at 5° N (black) and 5° S (gray) for $EXP_{FULL}$. Standard deviations and correlation coefficients between the hemispheres as well as the linear trends are displayed in the plot. Positive means anomalously strong STC according to STC index. (b) and (c) show the transport anomalies of the different branches of the STC integrated at 5° S and 5° N, respectively, for $EXP_{FULL}$. Solid gray/black line denotes STC strength, green shading surface branch, blue shading subsurface interior branch, and red shading WBC. Standard deviation of each branch and correlation coefficients between the surface branch and the sum of subsurface interior and WBC are displayed in each plot. The vertical dashed black lines indicate the strong El Niño events of 1982/1983, 1997/1998, and 2015/2016. Positive means northward transport for the branches and anomalously strong STC for STC index. STC = subtropical cell; SH = Southern hemisphere; NH = Northern hemisphere; WBC = western boundary current.

2004). $EXP_{FULL}$ shows a decreasing linear trend for the time period 1979–1993 and a reversed trend after that (Figure 5a). These trends are consistent with other model studies as well as observations (e.g., Capotondi et al., 2005; Lee & Fukumori, 2003; McPhaden & Zhang, 2002, 2004). For the targeted ENSO experiments ($ENSO_{ALL}$, $ENSO_{LIN}$, $ENSO_{NONLIN}$), neither of the two linear trends can be reproduced with a reasonable magnitude (Figure 5b). A detailed investigation of the linear trends is presented in section 3.2.4.

### 3.2. Hemispheric Separation of STC Variability

As the STC index may mask some of the variability by combining the NH and SH STCs, we now analyze the STCs in each hemisphere separately. Examining the Northern and Southern hemispheric contributions to the total $EXP_{FULL}$ STC transport reveals three fundamental differences (Figure 6a): (i) The NH STC displays interannual transport variability that is approximately 26% larger than that of the SH STC; (ii) the two STCs do not occur simultaneously. Rather, the NH STC leads the SH STC variations by 3 months; consequently, the behavior of the NH STC during El Niño/La Niña events strongly differs from the behavior of the SH STC; (iii) the decadal linear trend present in the STC index after 1993 is much more prominent in the SH STC.

Each of these hemispheric disparities and their physical origin are examined in detail in the following subsections utilizing the ENSO-targeted experiments. By comparing $ENSO_{ALL}$ to $EXP_{FULL}$, we are able to estimate to what extent the STCs can be reproduced by only forcing them with winds that are linked to ENSO. By means of $ENSO_{LIN}$ and $ENSO_{NONLIN}$, we can further draw conclusions about the physical mechanism behind the STC transports.

#### 3.2.1. Hemispheric Difference in Interannual Transport

We find that on interannual time scales, the variability of the NH STC (std: 5.7 Sv) is 26% larger than that of the SH STC (std: 4.5 Sv) in $EXP_{FULL}$ (Figure 6a). Looking at the individual branches of the STCs in $EXP_{FULL}$ reveals two things. First, the compensation between the subsurface interior and WBC branches is high in both hemispheres. Second, the compensation between the surface and the combined subsurface interior plus WBC branches is larger in the SH (corr: −0.75; Figures 6b and 6c). This alone would imply a stronger SH STC variability. However, even though the degree of compensation is slightly weaker in the NH, the STC branches themselves display a stronger variability, which leads to the increased variance of the NH STC. The exception is the WBC which displays similar variability in both hemispheres.

Here we investigate whether this hemispheric difference can be reproduced with the ENSO experiments. Analyzing the $ENSO_{ALL}$ experiment output reveals that the hemispheric difference as discovered in $EXP_{FULL}$

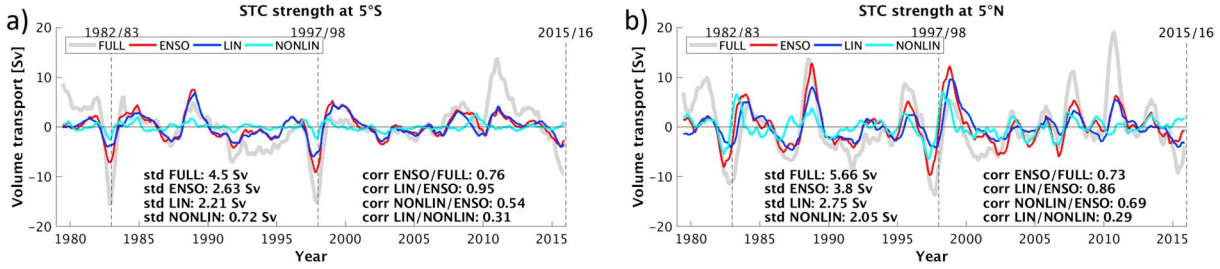


**Figure 7.** Anomalies of STC strength at (a) 5° S and (b) 5° N for all experiments. Gray color denotes $EXP_{FULL}$, red $ENSO_{ALL}$, blue $ENSO_{LIN}$, and cyan $ENSO_{NONLIN}$. Standard deviations and correlation coefficients between the experiments are displayed in the plot. The vertical dashed black lines indicate the strong El Niño events of 1982/1983, 1997/1998, and 2015/2016. Positive means anomalously strong STC. STC = subtropical cell; ENSO = El Niño-Southern Oscillation.

is reproduced reasonably well (Figure 7). On the basis that in $ENSO_{ALL}$, the NH STC varies with 44% more intensity than the SH STC, we first take a look at the $ENSO_{LIN}$ experiment which represents the common linear view of ENSO dynamics. The interannual variance of $ENSO_{LIN}$ transports is 24% larger at 5° N compared to 5° S. Thus, including the variability generated by $ENSO_{NONLIN}$ is synonymous with adding another 20% of hemispheric difference in interannual variance. This is taking into account the relative amplitudes of the $ENSO_{LIN}$ versus $ENSO_{NONLIN}$ transports.

The question can be raised why the $ENSO_{LIN}$ wind stresses generated stronger transport variability in the NH even though the wind stresses themselves vary stronger in the SH (Figure 2a). The answer is twofold. First, the surface branches are forced by the zonally integrated wind stresses, that is, even though the center of maximum variability is in the SH, the variability of the integrated wind stress along 5° N and 5° S is about the same in each hemisphere resulting in approximately equal Ekman variability. Second, the variability of the wind stress curl is stronger in the NH where it induces a stronger geostrophic flow (not shown). The resulting STC overturning transport, therefore, varies stronger in the NH.

We summarize this section by stating that the hemispheric disparity in the magnitude of the variance of the STCs can well be reproduced by forcing the STCs with ENSO-related winds only. This is due to both the $ENSO_{LIN}$ and $ENSO_{NONLIN}$ winds with comparable contributions.

### 3.2.2. Covariability of the STCs in Both Hemispheres

As discussed above, the $EXP_{FULL}$ STCs are not symmetric about the equator in terms of their transport variance. Focusing on the evolution of the STCs over time reveals that they are also not symmetric temporally, that is, they do not vary synchronously. The NH STC seems to lead the SH STC by 3 months (lagged corr: 0.75, Figure 6a). This lag is well captured by the $ENSO_{ALL}$ experiment (lag: 4 months, lagged corr: 0.87, Figure 8a), that is, ENSO-related winds appear to be responsible for the lag.

Based on the results of the previous section exhibiting a high compensation between the subsurface interior and the WBC transports in both hemispheres, we here combine these two branches to one branch and refer to it as the "subsurface branch." Looking for the source of the lag in $EXP_{FULL}$ (Figure 8b), we find that the STC subsurface branches in the NH and SH are fairly synchronous (corr: −0.69 at zero lag). The SH surface branch also displays a strong temporal similarity to the NH and SH subsurface branches, which is reflected by the correlation coefficients of 0.78 and −0.75 at zero lag, respectively (not shown). The NH surface branch, on the other hand, displays its strongest correlation with the SH surface branch when it leads by 7 months (corr: −0.66). This result indicates that the source of the lead/lag relationship is in the NH surface transports. The lead time of 7 months only applies to the NH STC surface branch, while the SH surface branch and the subsurface branches (interior + WBC) of both hemispheres act synchronously (zero lag). As the STC index is computed as surface-subsurface (NH) and subsurface-surface (SH) and the magnitudes of the surface and subsurface branches are similar, the lead-lag relationship of the STC indices is the average of the surface and subsurface lags. This yields the lag of 4 months for the STC index. Again, we find the same lead/lag relationships between all branches in $ENSO_{ALL}$ (Figure 8c), reinforcing our hypothesis that ENSO-related winds are the primary cause for the lag.

Comparison of the $ENSO_{ALL}$ experiment with $ENSO_{LIN}$ and $ENSO_{NONLIN}$ reveals a strong temporal consistency between the $ENSO_{ALL}$ and $ENSO_{LIN}$ transports in the SH, which suggests that the SH STC largely follows the linear recharge-discharge oscillator theory (see correlations in Figure 7a). In contrast, the

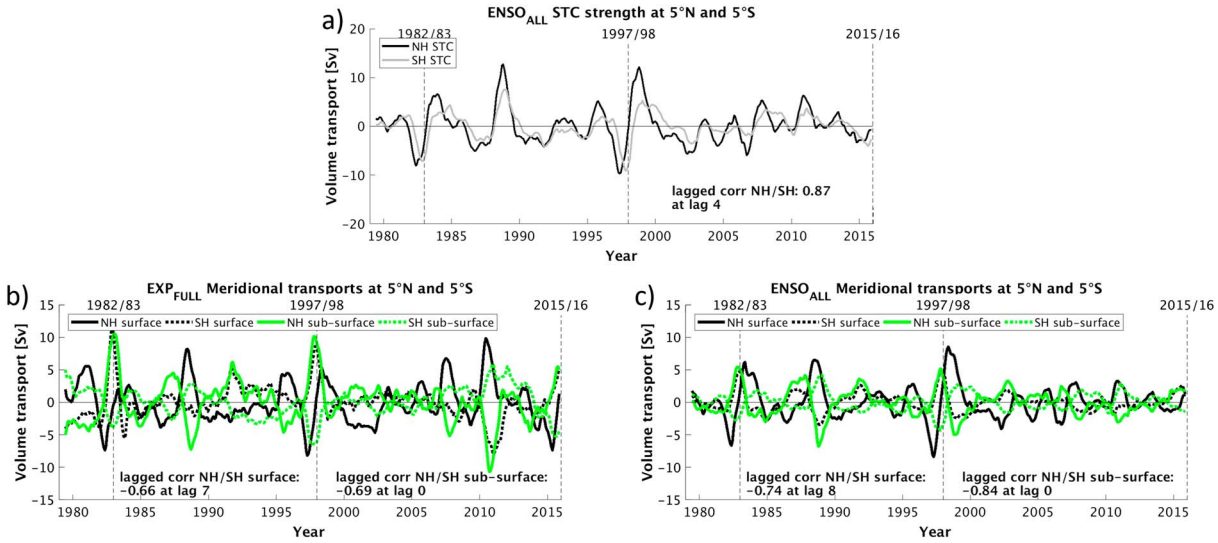


**Figure 8.** (a) Anomalies of STC strength at 5° N (black) and 5° S (gray) $ENSO_{ALL}$. Positive means anomalously strong STC according to STC index. Anomalies of the STC branches at 5° N (solid) and 5° S (dashed) for (b) $EXP_{FULL}$ and (c) $ENSO_{ALL}$. Black color denotes surface branch and green subsurface interior branch + western boundary current. Lagged correlation coefficients between the hemispheres are displayed in each plot. The vertical dashed black lines indicate the strong El Niño events of 1982/1983, 1997/1998, and 2015/2016. Positive means northward transport. ENSO = El Niño-Southern Oscillation; STC = subtropical cell; NH = Northern hemisphere; SH = Southern hemisphere.

influence of $ENSO_{LIN}$ is smaller in the NH STC where $ENSO_{NONLIN}$ also appears to play a prominent role (see correlations in Figure 7b). The cyclonic structure in the Northwestern tropical Pacific wind field (Figure 2b) induces Ekman transport that primarily affects the NH surface branch (e.g., McGregor et al., 2014). The time evolution of the $ENSO_{NONLIN}$ wind stresses is out of phase with the $ENSO_{LIN}$ wind stresses (see Figures 2b and 2c). Thus, the associated Ekman transports according to each forcing are out of phase, too. Consequently, the lead time of 8 months for the $ENSO_{ALL}$ surface branches is consistent with the lead time between the two wind forcing time series (7 months; Figure 2c). Plotting only the NH surface branch for all experiments confirms that the major contributor is the $ENSO_{NONLIN}$ experiment (Figure 9). $ENSO_{NONLIN}$ explains 77% of the variance of $ENSO_{ALL}$ and reaches clearly higher amplitudes than $ENSO_{LIN}$.

Summarizing this section, we can say that the 3-month lag between the NH STC and SH STC transport has its origin in the NH surface branch. Moreover, we know that ENSO-related winds are responsible for the phase shift. In particular, it is the cyclonic wind stress pattern over the North Western tropical Pacific corresponding to $ENSO_{NONLIN}$ that induces the lag between the hemispheres as seen in the fully forced STCs.

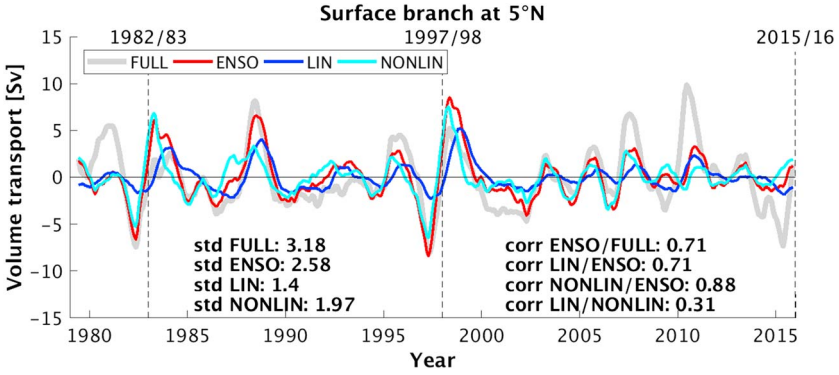


**Figure 9.** Anomalies of the Northern hemisphere subtropical cell surface branch at 5° N for all experiments. Gray color denotes $EXP_{FULL}$, red $ENSO_{ALL}$, blue $ENSO_{LIN}$, and cyan $ENSO_{NONLIN}$. Standard deviations and correlation coefficients between the experiments are displayed in the plot. The vertical dashed black lines indicate the strong El Niño events of 1982/1983, 1997/1998, and 2015/2016. Positive means northward transport. ENSO = El Niño-Southern Oscillation.

#### 3.2.3. Evolution of El Niño/La Niña Wvents

The phase difference between the STCs, as described in the previous section, causes them to play different roles during the development and decay of El Niño and La Niña events. The focus of this section is to analyze how the NH and SH STC evolve during the ENSO cycle. We distinguish between Eastern Pacific (EP) El Niños and Central Pacific (CP) El Niños following the "Nino" methodology set out by Yu and Kim (2013). Based on the Oceanic Nino Index (running 3-month mean SST anomaly averaged over the Nino3.4 region), we select the five strongest EP El Niños and the four strongest CP El Niños as well as the five strongest La Niña events from the 1979–2016 period to build event composites (Figures 2d and 2e). It is noted that four of the five strongest El Niño events in our time period are EP types and only one is a CP type. Our analysis therefore mainly focuses on the EP-type El Niño events. Again, the combination of the subsurface interior and the WBC transports is referred to as "subsurface branch" motivated by the compensating effect of the former two.

##### 3.2.3.1. EP-Type El Niño Events

We are first going to look at the average temporal evolution of the STCs in $EXP_{\mathrm{FULL}}$ during the EP-type El Niño events (Figure 10). Prior to an El Niño event peak, the NH surface branch has the biggest influence as its transport strongly decreases between January and September of the El Niño year, slowing the NH STC. Around the event peak (October–February), the NH STC becomes stronger again due to a rapid switch of the surface branch toward positive anomalies, despite an ongoing gradual decrease in transport of the subsurface branch. During this peak period, the SH STC transport reduces significantly due to reductions in the transports of both the surface and subsurface branches. It is noted that the STC reduction in both hemispheres is dominated by the surface branches whose changes are roughly double those of the subsurface branches in the respective time periods given the partial compensation of the subsurface interior transport through the WBC.

During the event decay and post event (March to November of the year after the event), the NH surface branch remains anomalously strong, while the SH surface branch changes sign and becomes strong, as well, further increasing the rate of the STCs. The NH subsurface branch adds to the STC strengthening later in the year (from August), while there is no effect of the subsurface branch in the SH integrated over this period. It should be noted that the enhanced STCs toward the end of the composite time frame are caused by the fact that El Niño events are mostly followed by La Niña events (Figure 2c). Hence, what is actually shown is the buildup phase of a subsequent La Niña event. Looking at the STC evolution of the individual EP El Niño events, depicted by the gray shading in Figures 10a and 10b, reveals that each event displays similar characteristics in each hemisphere to the mean during all ENSO phases.

The ENSO-forced ($ENSO_{\mathrm{ALL}}$) STC composites have a very similar temporal evolution to the fully forced simulation described above, although with reduced amplitudes (correlation coefficients of all composite time series lie between 0.77 and 0.98). This confirms that the ENSO forcing ($ENSO_{\mathrm{LIN}} + ENSO_{\mathrm{NONLIN}}$) as defined in our study is sufficient to reproduce the temporal evolution of the STC branches during El Ninño/La Niña events.

We now break the ENSO-driven STC down into linear and nonlinear ENSO changes to provide a better understanding of the drivers. Looking into the SH changes first, we find that the temporal evolution of the SH STC El Niño composite closely follows the linear ENSO theory ($ENSO_{\mathrm{LIN}}$). The nonlinear forcing ($ENSO_{\mathrm{NONLIN}}$) in the SH has a very minor impact on the SH STC. As to the NH STCs, both the $ENSO_{\mathrm{LIN}}$ and $ENSO_{\mathrm{NONLIN}}$ forcings play equivalent roles in the subsurface transports. At the surface, on the other hand, the transport is almost exclusively forced by the nonlinear wind stresses ($ENSO_{\mathrm{NONLIN}}$). Specifically, the switch of a weak to a strong NH surface branch just prior to the event peak coincides with the switch of the tropical Northwest Pacific anticyclone to a cyclone. Thus, nonlinear dynamics are required to explain the NH STC changes with maximum weakening occurring prior to the event peak.

##### 3.2.3.2. CP-Type El Niño Events

We also analyze the STC evolution during Central Pacific (CP) El Niños (dashed lines in Figure 10). The temporal evolution of the STC strength resembles the EP evolution, although with only about 60% of the amplitude for the STC minimum prior to the event peak in both hemispheres. After the peak time, the SH STC reaches the same strength for both El Niño types, while the NH STC regains much greater amplitude after CP El Niños. This strong regeneration after CP El Niño events is likely related to the development of La Niña events after every CP El Niño which is not the case for EP El Niño events.

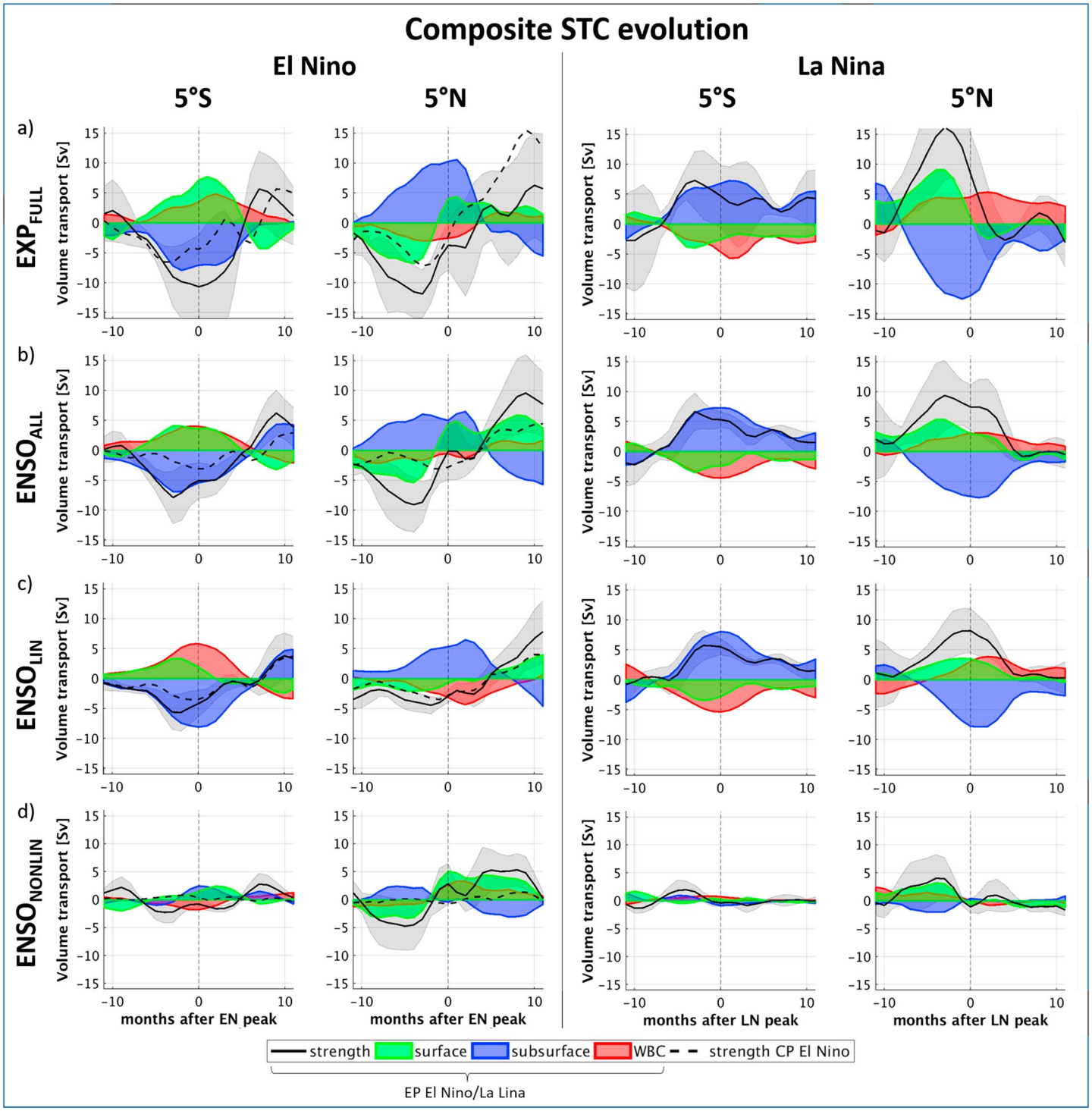


**Figure 10.** El Niño composites (1982/1983, 1987/1988, 1991/1992, 1997/1998, and 2002/2003, left column) and La Niña composites (1988/1989, 1998/1999, 1999/2000, 2007/2008, and 2010/2011, right column) of the anomalous branches of the STC at 5° N and 5° S for (a) $EXP_{FULL}$, (b) $ENSO_{ALL}$, (c) $ENSO_{LIN}$, and (d) $ENSO_{NONLIN}$. Solid black line denotes STC strength for EP El Nino/La Nina events, gray shading spread of single events, green shading surface branch, blue shading subsurface interior branch, red shading WBC, and dashed black line STC strength for CP El Niño events (1994/1995, 2004/2005, 2009/2010, and 2015/2016). The vertical dashed black line indicates the month of the event peak. Shown are the 11 preceding and following months of the event. A 3-month moving average has been applied to the data prior to analysis and plotting. Positive means northward transport for the branches and anomalously strong STC for the STC strength according to STC index. STC = subtropical cell; ENSO = El Niño-Southern Oscillation; WBC = western boundary current; CP = Central Pacific; EP = Eastern Pacific.

We find that the ENSO-driven part of the CP El Niños is almost exclusively driven by $ENSO_{LIN}$ winds, while $ENSO_{NONLIN}$ winds have no effect in either hemisphere. Figure 2e shows that the $ENSO_{NONLIN}$ winds are much weaker during the CP El Niño events explaining the minimal effect of these winds for the CP type of event. The strong regeneration of the STC strength at 5° N is not captured by the ENSO-related winds. This suggests that the difference between EP and CP El Niño events lies in the residual winds. It also suggests that the $ENSO_{NONLIN}$ wind stress pattern is predominantly related to EP El Niño and not CP El Niño events, which is corroborated by the minimal effect of $ENSO_{NONLIN}$ winds on the STC strength during CP El Niño events (cf. Figure 10d).

#### 3.2.3.3. La Niña Events

We now consider the evolution of the fully forced STCs during La Niña events (Figure 10). During the event growth period (January–September), the NH STC is largely responsible for the increase in STC transport. Both the surface and subsurface play a role in these NH STC changes, but as the surface transport lead those of the subsurface (i.e., NH surface transports peak 3 months prior to the event peak, while the subsurface transports peak 1 month prior to the event peak), they appear to be more important during this event growth phase. During the event peak (October–February), the NH surface branch returns to its mean value, while the NH subsurface branch is at its peak strengthening magnitude. The SH STC branches start strengthening around July midway through the event growth period and reach their peak magnitude in October. These SH STC changes occur in both the surface and subsurface maintaining a similar level through the event peak and decay in the following year. The ongoing strong SH STC goes back to the fact that La Niña events are usually followed by another La Niña event. In contrast to the SH STC, the NH STC returns back to normal within 4 months from the event peak.

Consistent with the El Niño composites, the ENSO-forced ($ENSO_{ALL}$) La Niña composites reproduce the temporal evolution of the $EXP_{FULL}$ composites in both hemispheres quite well. Looking to better understand the drivers of the STC changes, we break the ENSO-driven STC down into its linear and nonlinear components. We find that the SH STC is solely forced by $ENSO_{LIN}$ event composite winds, as $ENSO_{NONLIN}$ winds produce only very small changes of SH STC transport (Figure 10). For the NH STC, both linear and nonlinear winds play an essential role. In the pre-event period, the nonlinear winds induce a strong NH surface branch which enhances the transport of the NH STC. Then during the event peak (October–February), the linear winds become the dominant contributor, forcing a strong NH STC, while the STC contribution of the nonlinear winds returns to zero. During the event decay (March–May), the $ENSO_{LIN}$ winds diminish, and the NH STC returns to mean values.

#### 3.2.3.4. ENSO Summary

In summary, we can state that the temporal evolution of the SH STC largely follows the linear ENSO theory with zonal easterly (westerly) winds generating an accelerated (decelerated) STC. However, in contrast to theory, these changes are most prominent in the surface transports, which means that much less upper ocean heat content is lost from the equatorial region to the SH. This result is consistent with earlier studies (Kug et al., 2003; McGregor et al., 2014). Note again that the subsurface branch is defined as the sum of subsurface interior and WBC transports. The variation of the subsurface interior transport is still dominating the surface and WBC transport variations. While the linear component is important in the NH STC changes during ENSO events, as well, the nonlinear winds also play a prominent role. Their influence is most apparent during the buildup and decay phase of El Niño events, when the NH STC is largely forced by $ENSO_{NONLIN}$ winds. For La Niña events, the impact of $ENSO_{NONLIN}$ winds is most important during the buildup phase. In both cases, the nonlinear winds act to shift the peak of anomalous NH STC changes to earlier in the event evolution period.

### 3.2.4. Multidecadal Changes

Here we focus on understanding the longer-term variability of the STCs which are thought to be related to changes in the background state in which ENSO operates. Observational studies have looked at the decadal variability of the Pacific Ocean's dynamics by means of changes in the average state over decade-long time periods (e.g., McPhaden & Zhang, 2002, 2004). Accordingly, McPhaden and Zhang (2002) found a decrease of the STC convergence at 9° N and 9° S of about 0.5 Sv/year prior to the 1990s, followed by a substantial increase of about 1 Sv/year between the 1990s and the early 2000s (McPhaden & Zhang, 2004).

Our analysis is done at 5° latitude, but, when using the same time periods, we find qualitatively similar trends. The total STC (5° N + 5° S) decreases by 0.56 Sv/year between 1979 and 1993. It subsequently increases by 0.98 Sv/year between 1993 and 2008. However, McPhaden and Zhang (2004) did not

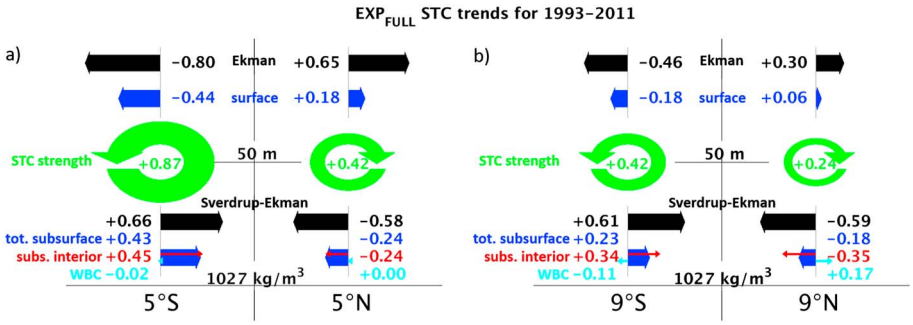


**Figure 11.** Linear trend of STC transports (Sv/year) at (a) 5° S and 5° N and (b) 9° S and 9° N in $EXP_{\mathrm{FULL}}$ for the period 1993–2011. The blue arrows indicate the trends of the surface branch (above circle) and the subsurface branch (below circle). The subsurface branch is separated into the subsurface interior trend (red) and the WBC trend (cyan). Also shown are the trends of the Ekman transport (above circle) and the geostrophic transport (below circle) derived from the wind forcing of $EXP_{\mathrm{FULL}}$ (black). The trend values are stated next to the corresponding arrows, where positive (negative) values represent an increase in northward (southward) transport. The circle indicates the trend of the STC strength and is the sum of the surface, subsurface interior, and WBC trends in their mean direction. The WBC trends at 5° S and 5° N are insignificant at the 90% confidence level. STC = subtropical cell; WBC = western boundary current.

consider the STC trend in each hemisphere separately, only discussing the combined trend of the pycnocline convergence (9° S–9° N).

Following from there, we take a look at the trends of the individual STCs. To rule out possible discrepancies in the first couple of model years right after the model initialization, we focus our analysis of the decadal STC changes on the period from 1993 to 2011. This period also captures the peak of the recent Pacific trade wind intensification (McGregor et al., 2018).

In $EXP_{\mathrm{FULL}}$, the decadal variability of the STCs at 5° N and 5° S appears asymmetric across the hemispheres (Figure 11a). The SH STC (+0.87 Sv/year) increases at double the rate as the NH STC (+0.42 Sv/year). The surface and subsurface interior branches change at a very similar rate within each hemisphere, although much stronger in the SH. The WBC does not appear to play any role in the STC spin-up in both hemispheres during this period. Specifically, we do not find a compensation of the subsurface interior and WBC branches at 5° latitude, as Lee and Fukumori (2003) and Capotondi et al. (2005) did at 9° latitude. The STC trends at 9° N and 9° S are generally weaker than at 5° N and 5° S. However, the fact that the difference in trends is also

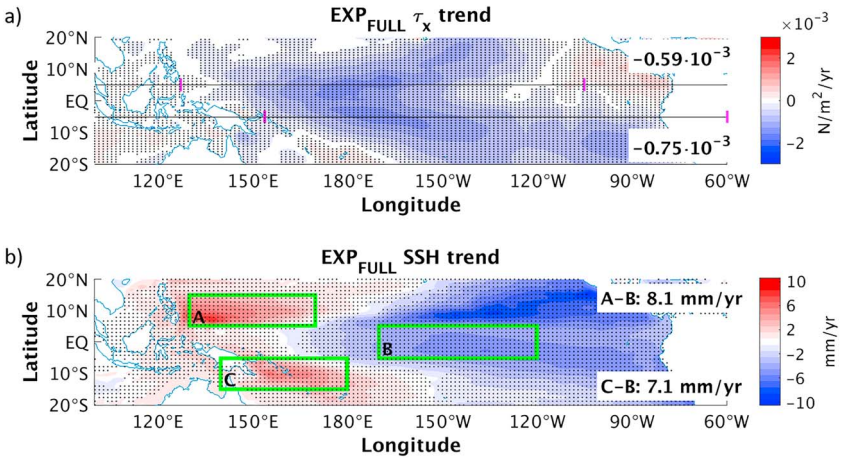


**Figure 12.** Linear trend for the period 1993–2011 in $EXP_{\mathrm{FULL}}$. (a) Zonal wind stress ($\tau_x$). The horizontal lines indicate the latitudes 5° N and 5° S. The numbers indicate the trends zonally averaged across the basin between the magenta lines. Red means increased eastward wind stress. (b) SSH. Boxes A and B are the same as used by Feng et al. (2010), while Box C is added to represent the Southern hemisphere trend. The numbers indicate the differences between the box averages. Red means increased sea surface height. In (a) and (b), the stippling indicates regions of significant trends at the 90% confidence level. SSH = sea surface height.

**Table 2**
*Regression Coefficients for the Multilinear Regression of Surface and Subsurface Subtropical Cell Branches Against Ekman and Geostrophic Transports at 5° S and at 5° N*

| | 5° S | | 5° N | |
|---|---|---|---|---|
| STC Branches | Ekman | Geo | Ekman | Geo |
| Surface | 0.83 | 0.33 | 0.36 | −0.02 |
| Subsurface | 0.03 | 0.64 | 0.31 | 0.72 |

seen at 9° N and 9° S (Figure 11b) gives us confidence that the meridional STC asymmetry is not dependent on the choice of latitude.

None of these trends in STC transport is produced by the targeted ENSO simulations (Figure 5b), a result which is consistent with past work (e.g., England et al., 2014). To better understand these changes, we estimate surface and subsurface transports from the linear trend of the surface wind stress forcing in $EXP_{\mathrm{FULL}}$ (Figure 12).

We expect the surface branches to be primarily forced by the overlying zonal wind stress and the accompanied Ekman transport. The zonal wind stress trend averaged across 5° N is 27% weaker than across 5° S (Figure 12a). The corresponding Ekman transports have according trends (Figure 11). However, the trends in the surface branches, in particular at 5° N, are much weaker than what Ekman theory suggests (72% weaker at 5° N; Figure 11).

As to the subsurface interior branch, Sverdrup theory suggests that this is forced by the basin-wide zonal pressure gradient which generates a geostrophic transport in meridional direction. The geostrophic transport can either be calculated directly from the SSH or as a residual by subtracting the Ekman transport from the Sverdrup transport, where the Sverdrup transport is derived from the wind stress curl. For both methods, the theoretically expected trend in geostrophic transport is approximately equal in both hemispheres (Figure 12b). However, the trend of the modeled subsurface interior branch at 5° N is only about half of that at 5° S (Figure 11).

Owing to the poor agreement between the modeled branches and the theoretical transports, we conducted a multilinear regression analysis to determine the relative contributions of the Ekman and geostrophic components to the modeled surface and subsurface STC branches (Table 2). We therefore solve the set of equation (3) for the Parameters a–d which quantify the Ekman and geostrophic components. A least squares estimation is applied in order to minimize the deviation of the observed data points from the fitted regression.

$$\begin{aligned} SFC &= \mathbf{a} \cdot T_{\mathrm{Ek}} + \mathbf{b} \cdot T_{\mathrm{Geo}}, \\ SUB &= \mathbf{c} \cdot T_{\mathrm{Ek}} + \mathbf{d} \cdot T_{\mathrm{Geo}}. \end{aligned} \tag{3}$$

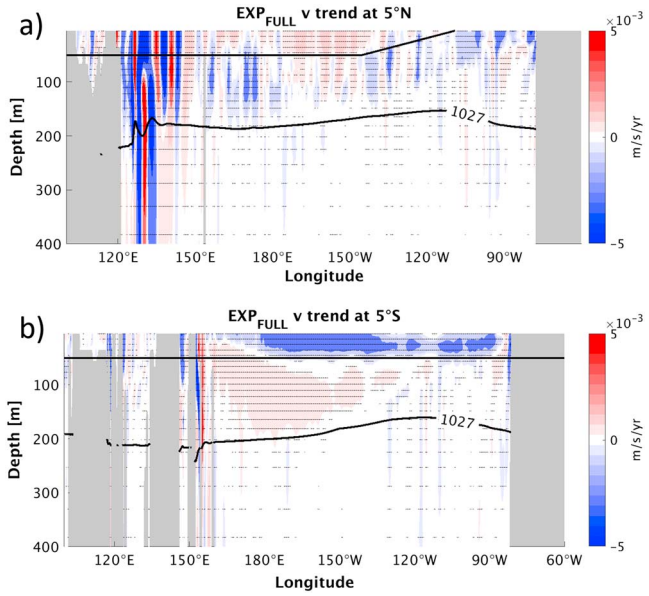


**Figure 13.** Linear trend of meridional velocity ($v$) for the period 1993–2011 in $EXP_{\mathrm{FULL}}$ across (a) 5° N and (b) 5° S. Red means increased northward velocity. The stippling indicates regions of significant trends at the 90% confidence level.

The analysis reveals that at 5° S, the ocean dynamics controlling these branches are consistent with linear and steady Ekman and Sverdrup theories. The surface branch is mainly driven by the Ekman component but is also partly influenced by the geostrophic transport, which explains the reduced trend of the modeled branch compared to that expected by calculations of Ekman transport. These findings are in accordance with Izumo (2005) who found a similar relation between theoretical and actual transports on interannual time scales.

At 5° N, however, Sverdrup theory cannot explain the weak modeled trends for both the surface and subsurface interior branch in $EXP_{\mathrm{FULL}}$. The modeled surface branch trend is only 28% of the trend in Ekman transport, while there is no geostrophic influence in the surface layer according to the multilinear regression analysis. The modeled trend in subsurface interior transport is 41% that of the geostrophic transport and in contrast to the SH, the NH subsurface transport appears to be strongly influenced by Ekman transport (Table 2).

To further investigate this unexpected behavior of the decadal trends at 5° N, we plot a section of the meridional flow showing its trend at each grid point across the basin at 5° N and 5° S (Figure 13). The plot shows that at 5° N, the linear trends do not coincide with the definition of the branches. Instead, positive and negative trends are highly mingled across the 50-m level. Because of the interference between the surface and subsurface branches, the linear trends of the two branches are partially cancelling.

This explains the strongly reduced trends that we find for the modeled STC branches at 5° N. The origin of this vertical interference is thought to be the high eddy activity across 5° N (Chen et al., 2015). At 5° S, on the other hand, the two branches can be clearly separated by means of the decadal trends.

Summing up, we find a strong hemispheric discrepancy for the decadal trends between 1993 and 2011. The trends at 5° S are in accordance with the driving forces and the theory. The strongly reduced trend of the NH STC can be traced back to enhanced vertical interference at 5° N. Our targeted experiments ($ENSO_{ALL}$, $ENSO_{LIN}$, and $ENSO_{NONLIN}$) cannot reproduce any trend implying that the multidecadal variability of the STC transport is not influenced by ENSO dynamics (Figure 5b).

## 4. Discussion and Conclusions

We have analyzed the shallow overturning circulation in the Pacific Ocean by means of a high-resolution ocean model forced by observed atmospheric conditions. Using a set of model experiments based on different wind forcings, we could relate the features of the STC variability to the oceanic and atmospheric processes that drive them. Our analysis leads to the following conclusions.

The temporal evolution of the interannual variability of the STCs can well be reproduced by forcing the ocean only with winds that are linearly and nonlinearly related to ENSO ($ENSO_{ALL}$). In terms of variance, $ENSO_{ALL}$ generates about two thirds of the STC transport forced by the total wind variability ($EXP_{FULL}$). This suggests that ENSO-related winds play an important role in driving the STCs on interannual time scales. Given the strong relationship between STC subsurface convergence and equatorial SST (e.g., Capotondi et al., 2005; Izumo, 2005), these winds evidently impact the climate of the tropical Pacific on these time scales.

The hemispheric difference in transport variance that was found for the STCs on interannual time scales appears to be induced by winds related to ENSO. The differing transport variance is nearly equally explained by the equatorial zonal wind stresses related to $ENSO_{LIN}$ and by the $ENSO_{NONLIN}$ wind stresses. In addition to the study by Kug et al. (2003) who divided the winds that are linearly related to ENSO into hemispherically symmetric and antisymmetric parts, we find the winds with a nonlinear relationship to ENSO almost double the hemispheric disparity in ocean transports. It is also noted that both Kug et al. (2003) and McGregor et al. (2014) focus on the upper ocean mass exchange (integrated from the surface to the pycnocline), while the present study examines how the rate of the NH and SH STC branches varies with the different forcings which ultimately changes the rate of upwelling at the equator.

We find a temporal asymmetry of the STC transports in the two hemispheres, whereby the NH STC leads the SH STC by 3 months. As most studies concentrate on the subsurface STC convergence which is proposed to occur in phase across the hemispheres (e.g., Chen et al., 2015; Cheng et al., 2007; Farneti et al., 2014; Izumo, 2005; Lbbecke et al., 2008; Schott et al., 2008), this temporal asymmetry has only briefly been mentioned before by Ishida et al. (2008). In their study, the authors highlight the temporal asymmetry between the NH and SH upper ocean meridional transports. They attribute the asymmetry to the NH WBC explaining that it lags the NH interior transport by several months while both transports are in phase (negative) in the SH. In the present study, however, we distinguish between the surface and the subsurface interior transports. This separation allows us to identify that the WBC and the subsurface interior transports are anticorrelated in both hemispheres (not only in the SH). Moreover, we find that rather than the NH WBC lagging the NH interior transports, it is the NH surface branch which leads both the NH subsurface interior and NH WBC branches. This circumstance ascribes particular importance to the NH surface transports, turning out to be the main actor in impacting the meridional mass exchange between the tropics and subtropics. The surface branch asymmetry is a consequence of the anticyclonic wind stress pattern over the Northwest tropical Pacific ($ENSO_{NONLIN}$). The fact that the timing of the $ENSO_{NONLIN}$ wind stress evolution is out of phase with the $ENSO_{LIN}$ wind stresses eventually results in the NH leading the SH surface branch by 8 months. Combined with the in-phase relationship of the subsurface and WBC branches, the total STC time lag is 3 months.

The time lag between NH and SH STCs leads to both cells playing different roles during the evolution of ENSO events. In this regard, the $ENSO_{NONLIN}$ winds critically influence the temporal evolution of the NH STC. This influence is reflected by a shift of the peak anomalous NH STC changes to 3 months earlier than when forced by the zonal wind stresses only. Since the SH STC is mainly forced by the $ENSO_{LIN}$ wind stresses, this means that the NH STC is the strongest (weakest) prior to the SH STC during El Niño (La Niña) events,

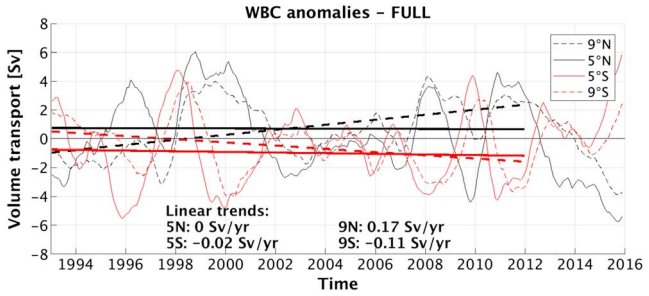


**Figure 14.** WBC transport anomalies and linear trends for the period 1993–2011 in $EXP_{\mathrm{FULL}}$. Solid black (red) lines indicate transport at 5° N (5° S); dashed black (red) lines indicate transport at 9° N (9° S). Positive means northward transport. The WBC trends at 5° N and 5° S are insignificant at the 90% confidence level. WBC = western boundary current.

which might attribute predictive skill to the NH STC. On a similar note, Widlansky et al. (2014) suggested predictive skill emerging from the tropical North Pacific anticyclone inducing prolonged low sea levels after strong El Niño events. Further to this, based on the differing evolution of the STCs in each hemisphere combined with each hemisphere's differing mean state, temperatures could act to modulate the temporal evolution of ENSO events and play a role in the apparent event seasonal synchronization.

During the recent (multi)decadal period, the SH STC appears to have played the most prominent role in the observed change of the tropical Pacific background state as the STC at 5° S increases at double the rate compared to 5° N. The reduced variability at 5° N relative to 5° S is not found to be due to reduced forcing but is related to the enhanced vertical interference which appears to be induced by the high eddy activity that is present across the basin at this latitude (Chen et al., 2015; Holmes et al., 2018). It is interesting to note that a similar hemispheric difference is found when the STCs are defined at 9° latitude, although the underlying physics are thought to be quite distinct from those occurring at 5° latitude, as this indicates the asymmetry is not sensitive to the latitude of the STC definition.

While it is currently unclear if this asymmetry would be apparent during past decadal changes, our results are in line with Luo and Yamagata (2001) who also ascribed a major role to the SH. Their mechanism is based on an atmospheric teleconnection from the Eastern equatorial Pacific to the subtropics and the subsequent advection of temperature anomalies back to the equator ($\bar{v}T'$). This is fundamentally different to the mechanism in the present study which is based on the varying overturning rate of the STCs ($v'\bar{T}$). We still need to better understand if the STC changes identified here influence the actual properties of the water upwelled in the equatorial region. However, as described in section 2.4, it appears that the major portion of pycnocline water that is transported toward the equator across 5° latitude actually originates from the subtropics and has to potential to modify the properties of the upwelled water.

Our results show that the (multi)decadal variability of the STC transport in either hemisphere is not driven by ENSO-related winds. The long-term trends in the volume transport of the STCs cannot be reproduced by our targeted ENSO experiments. Therefore, we can exclude this mechanism to be responsible for changes in the background state of the tropical Pacific ocean, consistent with England et al. (2014). In contrast to earlier studies (Farneti et al., 2014; McCreary & Lu, 1994), the observed wind forcing utilized in $EXP_{\mathrm{FULL}}$ and its decomposition for the other three experiments does not have clear distinctions between tropical and extratropical regions. However, in terms of the wind decomposition carried out, the $ENSO_{\mathrm{NONLIN}}$ experiment winds (Figure 2b) clearly has the strongest wind signature in the extratropical NH region. We find that while these winds drive STC interannual variability, they do not seem to play a role in driving the observed decadal STC changes.

Interestingly, the WBC in each hemisphere does not display a decadal trend during the 1993–2011 period. This is in contrast to analysis that was done for a similar period at 9° latitude, where the WBC and subsurface interior flow clearly oppose each other (e.g., Lee & Fukumori, 2003; Lee & McPhaden, 2008). We have repeated our analysis at 9° latitude, and our results are consistent with the above mentioned studies, that is, the decadal trends of the WBC and subsurface interior transport anomalies are counteracting each other. The reason for the missing trends of the WBC at 5° latitude can be attributed to the strong anomalies in the years 1995/1996 which are much weaker at 9° latitude (Figure 14). This implies that the interannually varying level of compensation between the WBC and the subsurface interior transports strongly affects the level of compensation on decadal time scales. The varying level of compensation between boundary and interior transports is thought to be very important for the tropical Pacific Ocean heat budget (Hazeleger et al., 2004).

Relating our results back to McPhaden and Zhang (2004), we find the same asymmetry of decadal STC trends at 9° latitude which is consistent with their study and can be inferred from their Figure 3a. We find that the reason for the reduced STC trend at 9° N is largely related to the reduced increase of the Ekman-driven surface branch (66% weaker, subsurface branch 22% weaker; Figure 11b). However, an additional component of the NH STC trend weakening originates from a stronger WBC at 9° N which poses a greater compensation to the subsurface interior transport (49%) compared to 9° S (32%). The intention here is to point out

the hemispheric difference in decadal STC trends and the potential impact of this difference on the tropical decadal variability rather than providing a physical explanation of the reduced trend in the NH. Hence, the proposed explanations are not meant to be definite but are rather a suggestion of possible causes for the difference in trends that have to be examined further in a future study.

Despite the SSH pattern of the tropical Pacific being closely related to the subsurface STC transport on interannual time scales (SSH leading by 2 months), this relationship appears to break down at longer time scales, in particular at 5° N. Thus, our results raise questions over the use of sea level measurements to monitor the decadal variability of the interior subsurface transport which is an integral part of the STCs (e.g., Feng et al., 2011). Given that the actual NH STC trend (Figure 11) is only half of that expected via calculation with the SSH gradients (cf. Figure 12b), our results suggest that caution should be placed in interpreting decadal STC changes derived from SSH. This in turn might lead to false conclusions on the amount of upwelled water at the equator and the associated SST and air-sea heat flux anomalies which determine the tropical Pacific climate.

We understand that the definition of the branches may introduce some uncertainty here. As can be seen from Figure 4b, the distinction between the mean surface and subsurface interior branches at 5° N seems to be not very clear. This is also represented in the high-regression coefficient between the surface branch and the Ekman transport (0.31). However, we have tested various definitions of the STC branches. Separating the surface and subsurface interior transports by an isopycnal surface instead of a constant depth level did not change the main results of this study. We have also tested numerous different definitions of the WBC, in particular at 5° N, some of which also include the recirculations and offshore branches. These definitions were based on various methodologies in order to find the longitude that best separates the WBC from the interior flow. Based on the correlation analysis as described in section 2.4, defining the WBC width by correlation with the core WBC transport is clearly physically meaningful. Thus, we believe that our definition of the STC branches provides a solid foundation for our analysis.

Previous studies have shown that spiciness anomalies that are generated in the subtropics and are largely transported with the STC branches have the potential to reach the equatorial Pacific where they can impact the heat exchange with the atmosphere (Schneider, 2000, 2004). Even though the decadal trend of the STC at 5° N is small, large amounts of water are transported toward the equator. Given the strong spiciness gradients found in each hemisphere, an open question is how the transport of spiciness anomalies of the NH and SH STC impacts the tropical climate. This will be the focus of future work.

**Acknowledgments**
This study was supported by the Australian Research Council (ARC) through Grant FT160100162, with additional support coming via the ARC Centre of Excellence in Climate System Science and the ARC Centre of Excellence in Climate Extremes. The model integrations were performed at the Australian National Computing Infrastructure (NCI) Facility. The ocean model output is available from the NCI facility. The Era-interim data is available from ECMWF (https://www.ecmwf.int/en/forecasts/datasets/archive-datasets/reanalysis-datasets/era-interim).

## References

Alexander, M., Blad, I., Newman, M., Lanzante, J., Lau, N.-C., & Scott, J. (2002). The atmospheric bridge: The influence of ENSO teleconnections on air-sea interaction over the global oceans. *Journal of Climate*, *15*(16), 2205–2231.

Barnett, T., Pierce, D., Latif, M., Dommenget, D., & Saravanan, R. (1999). Interdecadal interactions between the tropics and midlatitudes in the Pacific basin. *Geophysical Research Letters*, *26*(5), 615–618.

Bosc, C., & Delcroix, T. (2008). Observed equatorial Rossby waves and ENSO-related warm water volume changes in the equatorial Pacific Ocean. *Journal of Geophysical Research*, *113*, C06003. https://doi.org/10.1029/2007JC004613

Butt, J., & Lindstrom, E. (1994). Currents off the east coast of New Ireland, Papua New Guinea, and their relevance to regional undercurrents in the western equatorial Pacific Ocean. *Journal of Geophysical Research*, *99*(C6), 12,503–12,514.

Capotondi, A., Alexander, M. A., Deser, C., & McPhaden, M. J. (2005). Anatomy and decadal evolution of the Pacific subtropical-tropical cells (STCs). *Journal of Climate*, *18*(18), 3739–3758. https://doi.org/10.1175/JCLI3496.1

Chen, X., Qiu, B., Chen, S., Qi, Y., & Du, Y. (2015). Seasonal eddy kinetic energy modulations along the North Equatorial Countercurrent in the western Pacific. *Journal of Geophysical Research: Oceans*, *120*, 6351–6362. https://doi.org/10.1002/2015JC011054

Chen, H.-C., Sui, C.-H., Tseng, Y.-H., & Huang, B. (2015). An analysis of the linkage of Pacific subtropical cells with the recharge-discharge processes in ENSO evolution. *Journal of Climate*, *28*(9), 3786–3805. https://doi.org/10.1175/2015JC011054

Cheng, W., McPhaden, M., Zhang, D., & Metzger, E. (2007). Recent changes in the Pacific subtropical cells inferred from an eddy-resolving ocean circulation model. *Journal of Physical Oceanography*, *37*(5), 1340–1356. https://doi.org/10.1175/JPO3051.1

Chikamoto, Y., Mochizuki, T., Timmermann, A., Kimoto, M., & Watanabe, M. (2016). Potential tropical Atlantic impacts on Pacific decadal climate trends. *Geophysical Research Letters*, *43*, 7143–7151. https://doi.org/10.1002/2016GL069544

Davis, R. E., Kessler, W. S., & Sherman, J. T. (2012). Gliders measure western boundary current transport from the south Pacific to the equator. *Journal of Physical Oceanography*, *42*(11), 2001–2013. https://doi.org/10.1175/JPO-D-12-022.1

Dee, D. P., & Uppala, S. (2009). Variational bias correction of satellite radiance data in the ERA-Interim reanalysis. *Quarterly Journal of the Royal Meteorological Society*, *135*(644), 1830–1841. https://doi.org/10.1002/qj.493

Delworth, T. L., Rosati, A., Anderson, W., Adcroft, A. J., Balaji, V., Benson, R., et al. (2012). Simulated climate and climate change in the GFDL CM2.5 high-resolution coupled climate model. *Journal of Climate*, *25*(8), 2755–2781. https://doi.org/10.1175/JCLI-D-11-00316.1

England, M. H., Mcgregor, S., Spence, P., Meehl, G. A., Timmermann, A., Cai, W., et al. (2014). Recent intensification of wind-driven circulation in the Pacific and the ongoing warming hiatus. *Nature Climate Change*, *4*(3), 222–227. https://doi.org/10.1038/nclimate2106

Farneti, R., Dwivedi, S., Kucharski, F., Molteni, F., & Griffies, S. M. (2014). On Pacific subtropical cell variability over the second half of the twentieth century. *Journal of Climate*, *27*(18), 7102–7112. https://doi.org/10.1175/JCLI-D-13-00707.1

Fedorov, A. V., & Philander, S. G. (2001). A stability analysis of tropical ocean-atmosphere interactions: Bridging measurements and theory for El Niño. *Journal of Climate*, *14*(14), 3086–3101.
Feng, M., Bning, C., Biastoch, A., Behrens, E., Weller, E., & Masumoto, Y. (2011). The reversal of the multi-decadal trends of the equatorial Pacific easterly winds, and the Indonesian Throughflow and Leeuwin Current transports. *Geophysical Research Letters*, *38*, L11604. https://doi.org/10.1029/2011GL047291
Feng, M., McPhaden, M. J., & Lee, T. (2010). Decadal variability of the Pacific subtropical cells and their influence on the southeast Indian Ocean. *Geophysical Research Letters*, *37*, L09606. https://doi.org/10.1029/2010GL042796
Giese, B. S., Urizar, S. C., & Fukar, N. S. (2002). Southern hemisphere origins of the 1976 climate shift. *Geophysical Research Letters*, *29*(2), 1014. https://doi.org/10.1029/2001GL013268
Gordon, A. L., Susanto, R. D., & Ffield, A. (1999). Throughflow within Makassar Strait. *Geophysical Research Letters*, *26*(21), 3325–3328. https://doi.org/10.1029/1999GL002340
Gu, D., & Philander, S. G. H. (1997). Interdecadal climate fluctuations that depend on exchanges between the tropics and extratropics. *Science*, *275*(5301), 805–807. https://doi.org/10.1126/science.275.5301.805
Hazeleger, W., De Vries, P., & Van Oldenborgh, G. J. (2001). Do tropical cells ventilate the Indo-Pacific equatorial thermocline. *Geophysical Research Letters*, *28*(9), 1763–1766.
Hazeleger, W., Seager, R., Cane, M. A., & Naik, N. H. (2004). How can tropical Pacific Ocean heat transport vary? *Journal of Physical Oceanography*, *34*(1), 320–333. https://doi.org/10.1175/1520-0485(2004)034<0320:HCTPOH>2.0.CO;2
Hazeleger, W., Visbeck, M., Cane, M., Karspeck, A., & Naik, N. (2001). Decadal upper ocean temperature variability in the tropical Pacific. *Journal of Geophysical Research*, *106*(C5), 8971–8988.
Holmes, R., McGregor, S., Santoso, A., & England, M. H. (2018). Contribution of tropical instability waves to ENSO irregularity. *Climate Dynamics*, *52*, 1837–1855.
Hong, L., Zhang, L., Chen, Z., & Wu, L. (2014). Linkage between the Pacific Decadal Oscillation and the low frequency variability of the Pacific Subtropical Cell. *Journal of Geophysical Research: Oceans*, *119*, 3464–3477. https://doi.org/10.1002/2013JC009650
Ishida, A., Kashino, Y., Hosoda, S., & Ando, K. (2008). North-south asymmetry of warm water volume transport related with El Niño variability. *Geophysical Research Letters*, *35*, L18612. https://doi.org/10.1029/2008GL034858
Izumo, T. (2005). The equatorial undercurrent, meridional overturning circulation, and their roles in mass and heat exchanges during El Niño events in the tropical Pacific ocean. *Ocean Dynamics*, *55*(2), 110–123. https://doi.org/10.1007/s10236-005-0115-1
Izumo, T., Picaut, J., & Blanke, B. (2002). Tropical pathways, equatorial undercurrent variability and the 1998 La Niña. *Geophysical Research Letters*, *29*(22), 2080. https://doi.org/10.1029/2002GL015073
Jin, F.-F. (1997). An equatorial ocean recharge paradigm for ENSO. Part I: Conceptual model. *Journal of the Atmospheric Sciences*, *54*(7), 811–829.
Johnson, G. (2001). The Pacific Ocean subtropical cell surface limb. *Geophysical Research Letters*, *28*(9), 1771–1774. https://doi.org/10.1029/2000GL012723
Johnson, G. C., & McPhaden, M. J. (1999). Interior pycnocline flow the subtropical to the Equatorial Pacific Ocean. *Journal of Physical Oceanography*, *29*(12), 3073–3089. https://doi.org/10.1175/1520-0485(1999)029<3073:IPFFTS>2.0.CO;2
Kleeman, R., McCreary, J. P. Jr., & Klinger, B. A. (1999). A mechanism for generating ENSO decadal variability. *Geophysical Research Letters*, *26*(12), 1743–1746.
Kosaka, Y., & Xie, S.-P. (2013). Recent global-warming hiatus tied to equatorial Pacific surface cooling. *Nature*, *501*(7467), 403–407. https://doi.org/10.1038/nature12534
Kosaka, Y., & Xie, S.-P. (2016). The tropical Pacific as a key pacemaker of the variable rates of global warming. *Nature Geoscience*, *9*(9), 669–673. https://doi.org/10.1038/ngeo2770
Kug, J.-S., Kang, I.-S., & An, S.-I. (2003). Symmetric and antisymmetric mass exchanges between the equatorial and off-equatorial Pacific associated with ENSO. *Journal of Geophysical Research*, *108*(C8), 3284. https://doi.org/10.1029/2002JC001671
Kwon, Y.-O., Deser, C., & Cassou, C. (2011). Coupled atmosphere-mixed layer ocean response to ocean heat flux convergence along the Kuroshio Current Extension. *Climate Dynamics*, *36*(11-12), 2295–2312. https://doi.org/10.1007/s00382-010-0764-8
Large, W. G., & Yeager, S. G. (2009). The global climatology of an interannually varying air–sea flux data set. *Climate Dynamics*, *33*(2-3), 341–364. https://doi.org/10.1007/s00382-008-0441-3
Lbbecke, J., Bning, C., & Biastoch, A. (2008). Variability in the subtropical-tropical cells and its effect on near-surface temperature of the equatorial Pacific: A model study. *Ocean Science*, *4*(1), 73–88.
Lee, T., & Fukumori, I. (2003). Interannual-to-decadal variations of tropical-subtropical exchange in the Pacific Ocean: Boundary versus interior pycnocline transports. *Journal of Climate*, *16*(24), 4022–4042. https://doi.org/10.1175/1520-0442(2003)016<4022:IVOTEI>2.0.CO;2
Lee, T., & McPhaden, M. J. (2008). Decadal phase change in large-scale sea level and winds in the Indo-Pacific region at the end of the 20th century. *Geophysical Research Letters*, *35*, L01605. https://doi.org/10.1029/2007GL032419
Liu, Z., Philander, S. G. H., & Pacanowski, R. C. (1994). A GCM study of tropical-subtropical upper-ocean water exchange. *Journal of Physical Oceanography*, *24*(12), 2606–2623.
Lohmann, K., & Latif, M. (2005). Tropical Pacific decadal variability and the subtropical-tropical cells. *Journal of Climate*, *18*(23), 5163–5178. https://doi.org/10.1175/JCLI3559.1
Luo, J.-J., & Yamagata, T. (2001). Long-term El Niño-Southern Oscillation (ENSO)-like variation with special emphasis on the South Pacific. *Journal of Geophysical Research*, *106*(C10), 22,211–22,227.
Mantua, N., Hare, S., Zhang, Y., Wallace, J., & Francis, R. (1997). A Pacific interdecadal climate oscillation with impacts on salmon production. *Bulletin of the American Meteorological Society*, *78*(6), 1069–1079.
McCreary, J. P. Jr., & Lu, P. (1994). Interaction between the subtropical and equatorial ocean circulations: The subtropical cell. *Journal of Physical Oceanography*, *24*(2), 466–497.
McGregor, S., Gupta, A., & England, M. (2012). Constraining wind stress products with sea surface height observations and implications for Pacific Ocean sea level trend attribution. *Journal of Climate*, *25*(23), 8164–9176. https://doi.org/10.1175/JCLI-D-12-00105.1
McGregor, S., Gupta, A. S., & England, M. H. (2012). Constraining wind stress products with sea surface height observations and implications for Pacific Ocean sea level trend attribution. *Journal of Climate*, *25*(23), 8164–9176. https://doi.org/10.1175/JCLI-D-12-00105.1
McGregor, S., Spence, P., Schwarzkopf, F. U., England, M. H., Santoso, A., Kessler, W. S., et al. (2014). ENSO-driven interhemispheric Pacific mass transports. *Journal of Geophysical Research: Oceans*, *119*, 6221–6237. https://doi.org/10.1002/2014JC010286
McGregor, S., Stuecker, M. F., Kajtar, J. B., England, M. H., & Collins, M. (2018). Model tropical Atlantic biases underpin diminished Pacific decadal variability. *Nature Climate Change*, *8*, 493–498.

McPhaden, M. J., Zebiak, S. E., & Glantz, M. H. (2006). ENSO as an integrating concept in earth science. *Science*, *314*(5806), 1740–1745. https://doi.org/10.1126/science.1132588

McPhaden, M. J., & Zhang, D. (2002). Slowdown of the meridional overturning circulation in the upper Pacific Ocean. *Nature*, *415*(6872), 603–608. https://doi.org/10.1038/415603a

McPhaden, M. J., & Zhang, D. (2004). Pacific Ocean circulation rebounds. *Geophysical Research Letters*, *31*, L18301. https://doi.org/10.1029/2004GL020727

Meinen, C., & McPhaden, M. (2000). Observations of warm water volume changes in the equatorial Pacific and their relationship to El Nino and La Nina. *Journal of Climate*, *13*(20), 3551–3559. https://doi.org/10.1175/1520-0442(2000)013<3551:OOWWVC>2.0.CO;2

Meinen, C., & McPhaden, M. (2001). Interannual variability in warm water volume transports in the equatorial Pacific during 1993–99. *Journal of Physical Oceanography*, *31*(5), 1324–1345.

Meinen, C., McPhaden, M., & Johnson, G. (2001). Vertical velocities and transports in the equatorial pacific during 1993–99. *Journal of Physical Oceanography*, *31*(11), 3230–3248. https://doi.org/10.1175/1520-0485(2001)031<3230:VVATIT>2.0.CO;2

Montes, I., Colas, F., Capet, X., & Schneider, W. (2010). On the pathways of the equatorial subsurface currents in the eastern equatorial Pacific and their contributions to the Peru-Chile Undercurrent. *Journal of Geophysical Research*, *115*, C09003. https://doi.org/10.1029/2009JC005710

Neske, S., & McGregor, S. (2018). Understanding the warm water volume precursor of ENSO events and its interdecadal variation. *Geophysical Research Letters*, *45*, 1577–1585. https://doi.org/10.1002/2017GL076439

Newman, M., Alexander, M. A., Ault, T. R., Cobb, K. M., Deser, C., Di Lorenzo, E., et al. (2016). The Pacific decadal oscillation, revisited. *Journal of Climate*, *29*(12), 4399–4427. https://doi.org/10.1175/JCLI-D-15-0508.1

Nonaka, M., Xie, S.-P., & McCreary, J. (2002). Decadal variations in the subtropical cells and equatorial Pacific SST. *Geophysical Research Letters*, *29*(7), 1116. https://doi.org/10.1029/2001GL013717

Power, S., Casey, T., Folland, C., Colman, A., & Mehta, V. (1999). Inter-decadal modulation of the impact of ENSO on Australia. *Climate Dynamics*, *15*(5), 319–324. https://doi.org/10.1007/s003820050284

Schneider, N. (2000). A decadal spiciness mode in the tropics. *Geophysical Research Letters*, *27*(2), 257–260.

Schneider, N. (2004). The response of tropical climate to the equatorial emergence of spiciness anomalies. *Journal of Climate*, *17*(5), 1083–1095. https://doi.org/10.1175/1520-0442(2004)017<1083:TROTCT>2.0.CO;2

Schneider, N., Miller, A. J., Alexander, M. A., & Deser, C. (1999). Subduction of decadal North Pacific temperature anomalies: Observations and dynamics. *Journal of Physical Oceanography*, *29*(5), 1056–1070.

Schneider, N., Venzke, S., Miller, A. J., Pierce, D. W., Barnett, T. P., Deser, C., & Latif, M. (1999). Pacific thermocline bridge revisited. *Geophysical Research Letters*, *26*(9), 1329–1332.

Schott, F. A., McCreary, J. P. Jr., & Johnson, G. C. (2004). Shallow overturning circulations of the tropical-subtropical oceans. *Geophysical Monograph Series*, *147*, 261–304. https://doi.org/10.1029/147GM15

Schott, F. A., Stramma, L., Wang, W., Giese, B. S., & Zantopp, R. (2008). Pacific subtropical cell variability in the SODA 2.0.2/3 assimilation. *Geophysical Research Letters*, *35*, L10607. https://doi.org/10.1029/2008GL033757

Schott, F. A., Wang, W., & Stammer, D. (2007). Variability of Pacific subtropical cells in the 50-year ECCO assimilation. *Geophysical Research Letters*, *34*, L05604. https://doi.org/10.1029/2006GL028478

Spence, P., Griffies, S. M., England, M. H., Hogg, A. M., Saenko, O. A., & Jourdain, N. C. (2014). Rapid subsurface warming and circulation changes of Antarctic coastal waters by poleward shifting winds. *Geophysical Research Letters*, *41*, 4601–4610. https://doi.org/10.1002/2014GL060613

Stuecker, M. F., Timmermann, A., Jin, F.-F., McGregor, S., & Ren, H.-L. (2013). A combination mode of the annual cycle and the El Niño/Southern Oscillation. *Nature Geoscience*, *6*(7), 540–544. https://doi.org/10.1038/ngeo1826

Widlansky, M., Timmermann, A., McGregor, S., Stuecker, M., & Cai, W. (2014). An interhemispheric tropical sea level seesaw due to El Niño Taimasa. *Journal ofClimate*, *27*(3), 1070–1081. https://doi.org/10.1175/JCLI-D-13-00276.1

Wijffels, S., Firing, E., & Toole, J. (1995). The mean structure and variability of the mindanao current at 8°N. *Journal of Geophysical Research*, *100*(C9), 18,421–18,435.

Yu, J.-Y., & Kim, S. (2013). Identifying the types of major El Niño events since 1870. *International Journal of Climatology*, *33*(8), 2105–2112. https://doi.org/10.1002/joc.3575

Zhang, X., Sheng, J., & Shabbar, A. (1998). Modes of interannual and interdecadal variability of Pacific SST. *Journal of Climate*, *11*(10), 2556–2569. https://doi.org/10.1175/1520-0442(1998)011<2556:MOIAIV>2.0.CO;2

Zhao, M., Hendon, H., Alves, O., Liu, G., & Wang, G. (2016). Weakened Eastern Pacific El Niño predictability in the early twenty-first century. *Journal of Climate*, *29*(18), 6805–6822. https://doi.org/10.1175/JCLI-D-15-0876.1

Zilberman, N., Roemmich, D., & Gille, S. (2013). The mean and the time variability of the shallow meridional overturning circulation in the tropical south Pacific Ocean. *Journal of Climate*, *26*(12), 4069–4087. https://doi.org/10.1175/JCLI-D-12-00120.1